VOL. 34, Nº 2

DICIEMBRE 2012

ISSN 0717-2915

Revista Journal SELPER

Cayena

Imagen de satélite LandSat 8 OLI

REVISTA JOURNAL

SOCIEDAD LATINOAMERICANA DE PERCEPCION REMOTA Y SISTEMAS DE INFORMACION ESPACIAL• SOCIEDADE LATINO-AMERICANA EM SENSORIAMENTO REMOTO E SISTEMAS DE INFORMAÇAO ESPACIAL• LATINAMERICAN SOCIETY ON REMOTE SENSING AND SPACE INFORMATION SYSTEM

SELPER

VOL. 34 Nº 2 | Diciembre 2012 | ISSN 0717-2915

FOTO PORTADA

Cayena

Imagen de satélite Landsat 8 OLI, resolución espacial 30 metros, en composición 4,3,2 - RGB, de la ciudad de Cayena tomada el 26 de julio de 2014. Los sectores que se destacan son: Matoury, Remire Montjoly y Roura.

EJEMPLAR DE DISTRIBUCION GRATUITA. PROHIBIDA SU VENTA

DIRECTORIO SELPER, SEDE Francia 2012 - 2014

Institut de recherche pour le développement Le Sextant

44, bd de Dunkerque, CS 90009 - 13572 Marseille cedex 02

Tél. 33 (0)4 91 99 92 00 - Fax 33 (0)4 91 99 92 22

selper.internacional@gmail.com

PRESIDENTE

Laurent Durieux

Francia

VICE–PRESIDENTE

Marie José Lefevre Fonallosa

Francia

VICE-PRESIDENTE

Silvia Casas

México

VICE-PRESIDENTE

Luz Angela Rocha

Colombia

RESPONSABLE DE DIVULGACIÓN ELECTRÓNICA

Fabián Lozano García

Mexico

COMITÉ DE RELACIONES INTERNACIONALES

Luz Angela Salamanca (Colombia)
Presidente interina
Laurent Durieux – Francia
Pedro Luis García Pérez - Cuba
Pedro Martínez Fernández - Cuba
Olga Piedad Rudas - Colombia
Anyul del Pilar Mora - Colombia
Luis Geraldo Ferreira - Brasil
Washintong Franca Rocha - Brasil
Victor Barrena - Perú

COMITÉ EDITORIAL

María Cristina Serafini (Argentina)
Presidente
Miriam Esther Antes – Argentina
Fabián Lozano – México
Leila María Fonseca – Brasil
Jorge Martín Chiroles - Cuba
Francisca Celia González - Argentina
Freddy Flores – Venezuela

COMITÉ DE EDUCACIÓN

Maria Antonia García Cisnero (Cuba)
Presidente
Luz Angela Rocha Salamanca - Colombia
Laura Delgado - Venezuela
Ethel Rubín de Celís Llanos - Perú
Josselisa Ma. Chávez - Brasil

COMITÉ DE PROYECTOS INTERNACIONALES

Paulo Roberto Martini (Brasil)
Presidente
Christopher Charron – Francia
Alfredo Cuello – Argentina
Miembro del ISPRS

CAPÍTULOS CONSTITUIDOS

ARGENTINA
Miriam Esther Antes
Universidad Nacional de Luján (PRODITEL)
Fuerza Aérea Argentina (CSR)
Cruce Rutas 5 y Ex. 7 (6700)
Luján, Buenos Aires, Argentina
Tel: 54 - 2323- 420380 - int. 248
Fax: 54 - 2323- 425795
E-mail: selperargentina@gmail.com

BOLIVIA
José Luis Liseca
Carrera de Topografía y Geodesia
Facultad Técnica
Universidad Mayor de San Andrés
Av. Arce 2299 1º Piso
La Paz, Bolivia
Tel.: 591-2-2441401
E-mail: jlisec@hotmail.com

BRASIL
Laércio Massuru Namikawa
INPE
Av. Dos Astronautas 1758, Sao José dos Campos
San Pablo, Brasil
Tel: 55 - 12-39456000
E-mail: laercio@dpi.inpe.br

CHILE
Héctor Gutiérrez Méndez
Centro Nacional de Información Aeroespacial
Antonio Varas 175
Oficina 310. Providencia
Tel: 562 -2362714
E-mail: hector.gutierrez@cenia.cl

COLOMBIA
Luz Angela Rocha Salamanca
Carrera 30 No. 48-51 Edificio IGAC-CIAF Of. 212
Bogotá D.C., Colombia
Tel: 57-1-369-4096
Fax: 57-1-369-4096
E-mail: lrochas@selper.org

CUBA
Pedro Luis García Pérez
Sede UNAICC, Humboldt No. 104,
Esquina a Infanta, Vedado, La Habana, Cuba
Telf.: (5 37) 8363447
E-mail: lgarcia@ch.unaicc.cu

ECUADOR
Cor. Ricardo Urbina
CLIRSEN
Edif. Instituto Geográfico Militar, Piso 4
Seniergues s/n y Paz y Miño
Apartado Postal 17-08-8216

GUATEMALA
Carlos Alberto Duarte
Ingeniería Virtual
Ruta 4, 6-49 Zona 4, Oficina 14
Ciudad de Guatemala (01004), Guatemala
Tel: 502 - 334-1039/4038
Fax: 502 - 331-9390
E-mail: chduarte@hotmail.com

GUYANA FRANCESA
Laurent Polidoril
Directeur de Recherche IRD / US ESPACE 140
Institut de Recherche pour le Développement (ex-ORSTOM)
Route de Montabo - BP 165 - 97323 Cayenne cedex
Tel. (+594) 594 29 92 81
Fax (+594) 594 31 98 55
E-mail:polidori@cayenne.ird.fr

MÉXICO
Jean Francois Mass
UNAM Campus Morelia
Morelia, Michoacan, México
E-mail: jfmas@ciga.unam.mx

FRANCIA
Marie José Lefevre Fonollosa
CNES
18 avenue Edouard Belin, 31401 Toulouse Cedex 9
Tél : 3305 61 27 4283
Fax : 3305 61274842
E-mail: marie-jose.lefevre @cnes.fr

URUGUAY
Antonio Alarcón
Servicio de Sensores Remotos Aeroespaciales Fuerza Aérea Uruguaya
Ruta 101 s/n Km. 19500
Carrasco, Canelones, Uruguay
Tel.: 598 -2 601 4083
Fax: 598 -2 601 4090
E-mail: aalarconv@hiotmail.com

VENEZUELA
Ramiro Salcedo
Centro de Procesamiento Digital del Instituto de Ingenieria en Caracas
Apdo. Postal 40200 / Caracas, Venezuela
Tel/fax: 58 - 212 - 903 -4682
E-mail: ramiros@fii.org

PERÚ
Victor Barrena Arroyo
Universidad Nacional Agraria La Molina
Av. La Universidad s/n
La Molina, Lima, Perú
Tel / Fax: 51-1-349-5647 anexo 232/349-2041

CAPÍTULOS EN FORMACIÓN

PARAGUAY
Sergio M. Burgos Sosa
IPPA
Dr. César Sánchez 431
San Lorenzo, Paraguay
Tel/Fax: 595- 21-574909
Email: smburgos@highway.com.py

CAPÍTULOS ESPECIALES

ALEMANIA
Klaus Reiniger
DLR
D-8031 Oberpfaffenohfen
Alemania
Tel: 49- 8153- 281.189
Fax: 49- 8153- 281.443

CANADÁ
Fritz P. Dubois
25 Nidland
Crs Nepean Ontario Kh2-8n2
Ontario, Canadá
Tel: 613- 596-4164
Fax: 613- 723-9626

ESPAÑA
José L. Labrandero
Consejo Superior de Investigaciones Científicas (CSIC)
Pinar 25- Madrid 28006, España
Tel: 34- 411.10.98
Fax: 34- 562.55.67

HOLANDA
Carlos Valenzuela
ITC
350 Boulevard 1945, P.O.X. 6. 7500 AA
Enschede, Holanda
Tel.: 31 53 874-444
Fax: 31 53 874-400

ITALIA
Francesco Sarti
ESA/ESRIN
Via Galileo Galilei, s/n
I-00044 Frascati, Italia
Tel: 39 - 694180409
Fax: 39 - 694180602
E-mail: Francesco.Sarti@esa.int

Maurizio Fea
via Alessandro Poerio, 49
00152 Roma
tel/fax: +39065880581
móvil: +393281771383
E-mail: maufea@gmail.com

USA
Patricia M. Ravelo
SPOT
Estados Unidos
Tel: 1-800-ask-spot ext. 137
Fax: 703-648.1813
E-mail: ravelo@spot.com

COMITÉ EDITORIAL

María Cristina Serafini (Argentina)
PRODITEL
Universidad Nacional de Luján
Cruce rutas 5 y ex 7
(6700) Luján, Buenos Aires, Argentina
Tel: 54-2323-423171 int 248
Fax: 54-2323-425795
E-mail: proditel@mail.unlu.edu.ar

Miriam Esther Antes (Argentina)
PRODITEL
Universidad Nacional de Luján
Cruce rutas 5 y ex 7
Luján, Buenos Aires, Argentina
Tel: 54-2323-423171 int 248
Fax: 54-2323-425795
E-mail: selperargentina@gmail.com

Leila María Fonseca (Brasil)
INPE
Av. Dos Astronautas 1758, Sao José dos Campos, Sao Paulo, Brasil
Tel: 55 - 12-39456000
E-mail: leila@dpi.inpe.br

Fabián Lozano (Mexico)
Instituto Tecnológico y de Estudios Superiores de Monterrey
Av. Euganio Garza Sada # 2501 sur, Col. Tecnológico, Monterrey, Nuevo León, México
Tel: 52 - 81 - 8358 - 1400 ext 5275
Fax: 52 - 81 - 8358 - 6280
E-mail: dflozano@itesm.mx

Jorge Martín Chiroles (Cuba)
E-mail: ciencia@geocuba.com.cu

Francisca Celia González (Argentina)
Universidad Nacional del Sur
Departamento de Geología
San Juan 670 (8000)
Bahía Blanca, Argentina
Tel: 54 - 291 - 459 5102 - int. 4360
Fax: 54 - 291 - 459 5127
E-mail: ghgonzal@criba.edu.ar

Freddy Flores (Venezuela)
Fundación Instituto de Ingeniería
Carretera Vieja de Baruta, Sector Sartenejas, Urb. Monte Elena II
Caracas, Venezuela
Tel: 58 2-903 4661-4610
Fax: 58 2- 903 4780
E-mail: freddyf@fii.org

COMITÉ DE EVALUADORES

Maurizio Fea
(ASI - Italia)
Héctor del Valle
(CENPAT - Argentina)
Walter Sione
(UNLu - Argentina)
Gustavo Buzai
(UNLu - Argentina)

Editado por: SELPER Internacional
Universidad Nacional de Luján
Rutas 5 y ex 7, (6700) Luján - Bs. As. ARGENTINA

EJEMPLAR DE DISTRIBUCIÓN GRATUITA PROHIBIDA SU VENTA

PLAN EDITORIAL SELPER 2012 - 2014

PLAN EDITORIAL SELPER

A partir de las decisiones adoptadas en el marco del XIII Simposio Latinoamericano de Percepción Remota y Sistemas de Información Espacial, llevado a cabo en La Habana, Cuba, en setiembre de 2008, la edición de la Revista SELPER está disponible en la página de nuestra Sociedad: http://www.selper.info.

En esta oportunidad hacemos llegar la publicación del volumen 34 Número 2., donde se incluyen trabajos que han sido presentados en el XIV Simposio Latinoamericano de Percepción Remota y Sistemas de Información Espacial (SELPER), desarrollado en Cayena, Guyana Francesa, en noviembre de 2012.

NORMAS PARA LOS AUTORES

Los artículos recibidos serán enviados a tres (3) expertos en la temática para su revisión. Los trabajos aprobados serán publicados en estricto orden, de acuerdo a las fechas de llegada de las contribuciones.

Los idiomas oficiales SELPER son: Español, Portugués e Inglés.

Los trabajos deberán estructurarse contemplando las siguientes secciones:

a) Título del trabajo. Nombre de los autores y direcciones completas

b) Resumen (no más de 150 palabras) indicando al final las palabras claves. Deberá incluirse en Español o Portugués, además de Inglés

c) Introducción

d) Objetivos

e) Metodología empleada y materiales

f) Resultados obtenidos

g) Conclusiones

h) Bibliografía: sólo se incluirá la citada en el texto. Se indicarán los autores, por orden alfabético, año, título, revista o medio donde fue publicado, incluyendo volumen y páginas, cuando corresponda.

Los títulos y subtítulos de cada sección deberán estar claramente indicados (ya sea con numeración o tamaño de letras). Las tablas, fotos y figuras deberán ser suficientemente nítidas, llevar un título y estar numeradas en forma consecutiva.

Se deberá enviar una copia del trabajo en formato Word y una copia papel. La extensión total del trabajo no deberá superar las 12 páginas, (DIN-A4).

Los trabajos se enviarán a: editorial@selper.org

Characterization and distribution of the land cover change in Mexico between 2005- 2010 based on automated detection with 250m MODIS images

Ricardo Magdaleno Llamas
René Roland Colditz

National Commission for the Knowledge and Use of Biodiversity (CONABIO), Avenida Liga Periférico-Insurgentes Sur 4903, Col. Parques de Pedregal, Tlalpan, 14010, México D.F.
rllamas@conabio.gob.mx, rcolditz@conabio.gob.mx

ABSTRACT

Monitoring of environmental variables is a great challenge to derive reliable products that characterize the Earth´s surface in an accurate manner. Land cover and its changes are valuable components in map making that focus on climate change studies and human impact on the environment. The North America Land Change Monitoring System (NALCMS) is an initiative which conducts land cover and change mapping for Mexico, United States and Canada. This trinational project is coordinated by the Commission for Environmental Cooperation (CEC) which facilitates the work among countries. For Mexico, the change mask 2005-2010 has been recently completed and will be combined with similar national products of the other countries to detect changes across North America. This work describes how the mask for Mexico was generated by means of MODIS monthly composites from 2005 and 2010, assessing biannual differences between spectral bands, NDVI and two textural features. Landsat TM 5 images were also used to develop a training data set through visual change detection over central and northern portions of Mexico where most of the Landsat tiles were available. This visual-made training set was applied to calibrate the change detection algorithm. The paper shows the results for automated change detection and validation that focused on the correct delineation of detected change areas in order to assess final confidence. During validation, all polygons identified as change were assigned to six categories. In addition analysis of highlights case studies is presented.

Keywords: MODIS, Land cover, Change detection, Change characterization, Spatial distribution.

1. INTRODUCCION

The coverage on the surface of the Earth and its changes have been widely studied since it has a main importance concerning to understanding the evolution of the societies, the development of models in order to study local and global scale phenomena, and monitoring how human activities impact on the planet. This sort of studies includes forest disturbance mapping (Masek et al. 2008, Pouliot et al. 2009), inventories (Feranec et al. 2010), resource management of protected areas (Fraser et al. 2009) and planning (Manonmani and Suganya, 2010). In this sense, the North American Land Change Monitoring System (NALCMS) provides information about the land cover at continental scale and is looking forward to developing annual land cover products and change detection maps between specific periods. NALCMS is a trinational initiative coordinated by the Commission for Environmental Cooperation (CEC) which facilitates projects between Mexico, United States and Canada. Since the land cover map of 2005 was published in 2010, the project aims to develop a change mask between 2005 and 2010 in order to update the initial 2005 map. As each country involved in the project develops its own change mask, for the Mexican portion the National Institute for

Statistics and Geography (INEGI), the National Commission for Knowledge and Use of Biodiversity (CONABIO), and National Forestry Commission (CONAFOR) generated and assessed the national product which will be merged with US and Canada maps. The Mexican change map was obtained by an automated process based on monthly MODIS composites of bands 1 to 7 that were produced by the Canada Centre for Remote Sensing (CCRS) for the three countries (Latifovic et al. 2012). Additional data such as the NDVI and texture filters were generated by CONABIO. The method applied for change detection regards spectral differences between a comparable set of features from 2005 and 2010, matching data from the same month. This is a common technique for change detection(Muchoney and Haak. 1994, Healey et al. 1994 among others). Only extreme differences between both years were considered to find the best change patterns. In order to choose the best lower and upper thresholds for these extreme differences, the values were divided into different combination of quantiles and amounts of features. These combinations were faced against a training data set developed with Landsat 5TM images over the central and northern portions of Mexico, where Landsat data are available for both years and cloud free data offer the best chance for visual land change identification. The comparison with training data produced different indices and the combination of features and quantiles which performed best was chosen as the final change mask for Mexico.

Even though different studies have been developed in Mexico at local and regional scale (Berlanga-Robles and Ruiz-Luna, 2002, Mass, 1999), just a few national efforts are available, (INEGI 2009, Mas et al. 2004, Couturier et al. 2012). The main advantage of the NALCMS change mask is that it is generated by an automated algorithm which avoids human influence derived from visual analysis, besides this method allows detect changes over almost two millions of square kilometers in so much less time that required by human efforts.

However, resulting change polygons must be reviewed in order to assess the accuracy of the final product and its confidence in different regions. This paper focuses on the outputs of validation that are presented in Colditz et al. (2012), and characterize the type of change as well depicts its distribution over Mexico. Three study cases are also analyzed due to the reliable impact they have on the land surface. Urban sprawl in Cancun, on the Yucatan peninsula in south- east (Veloz Avilés, 2011); and Monterrey in the northeast of Mexico can be related to fast economic growth in those areas. Water level changes at Alvaro Obregon reservoir in the northwest illustrate how the algorithm works and why its outputs have to be validated.

2. METHOD

The process of change detection mask was based on normalized monthly composites ofMODIS images of band 1 to 7 (blue to short wave infrared) for the entire country, as well as the NDVI and textural features generated from normalized data. This process is based on the assumption that both years correspond temporally (Colditz et al. 2012). The difference for each feature was computed between each composite from 2010 to its corresponding one from 2005. In order to evaluate the best set of features and the most suitable thresholds of extreme values related to well-known change areas, many runs were tested and the outputs were compared with training data developed by visual analysis on Landsat5 TM images. The most similar combination of inputs and difference values divided into quantiles were established as the final change mask.

2.1Training data

A set of Landsat5 TM images of April and October from 2005 and 2010 was downloaded in order to evaluate changes during dry season and at the end of the rainy season, respectively. Only images for the central and northern portions of Mexico were available. The final composes of 74 pairs images of 133 required images to cover entire Mexico, Figure 1. Finally, areas evaluated as real change by an analyst were digitized if the polygon detected was persistent in both dry and rainy season.

Thus the identification of land cover changes in the final reference map served to train the algorithm in order to find the best combination of features, lower and upper quantiles and number features aggregated to flag a pixel as change and get the best correspondence between both products.

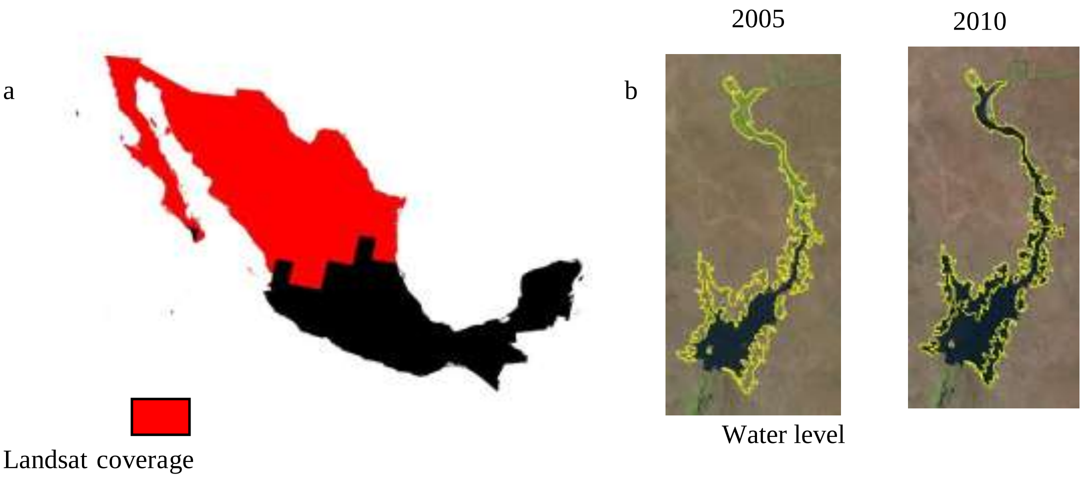

Figure 1. a) Lansat5 TM images availability over the central portions of Mexico is shown in red, the black patch corresponds to area where no cloud free images were found. b) Polygon digitized as change is shown over a water reservoir, water lever difference is clearly visible

2.2 Change detection

Once the reference map was finalized, many attempts to find the best parameters ofbiannual difference were tested. If we consider that no change between both years means values close to zero, so the extreme values of the difference histogram could be considered as potential change. Besides aggregation of features was taking into account due to some land cover changes are not recorded by many spectral bands, thus the portion of features from the entire set which match the best with the reference map was established as frequency of change flagged in each pixel.

In this sense, different runs considering lower and upper quantiles combinations demonstrated that the best result was obtained with 120 features, including 7 bands of each month, NDVI and two derived textural features (Sobel and Laplace) based on NDVI. The most appropriate lower and upper thresholds were 1 and 99% quantiles respectively, and the frequency of extreme values for those quantiles was 28. The output was compared to the reference map using the phi-coefficient. For the preliminary change mask, a phi of 0.2559 was reported. Further processing exclude areas well-known as no change due to phenological stages in agricultural zones and smalls patches of remaining clouds among others.

The final processing step applied a minimum mapping unit (MMU) of 4 pixels in order to show only representative changes. The area detected as change is 780,462.5ha (0.39% of the total land surface) where well-known change areas were excluded, and 698,956.3ha (0.35%) with applying the MMU (Colditz et al. 2012). The mask without MMU represents the maximum potential change over Mexico between 2005 and 2010 in Figure 2.

2.3 Validation

Once the final change mask was delineated Figure 2, validation consisted about identify each single pixel inside polygons assessed by the algorithm. This process was conducted by an analyst work and classification as change or no change laid on his criterion. Visual analysis was made contrasting monthly MODIS composites generated with RGB combination of 721 spectral bands. As it was done with reference map, images from April at dry season and October at the end of the rainy season were employed for this analysis looking forward detecting persistence change in both cases for 2005 and 2010.

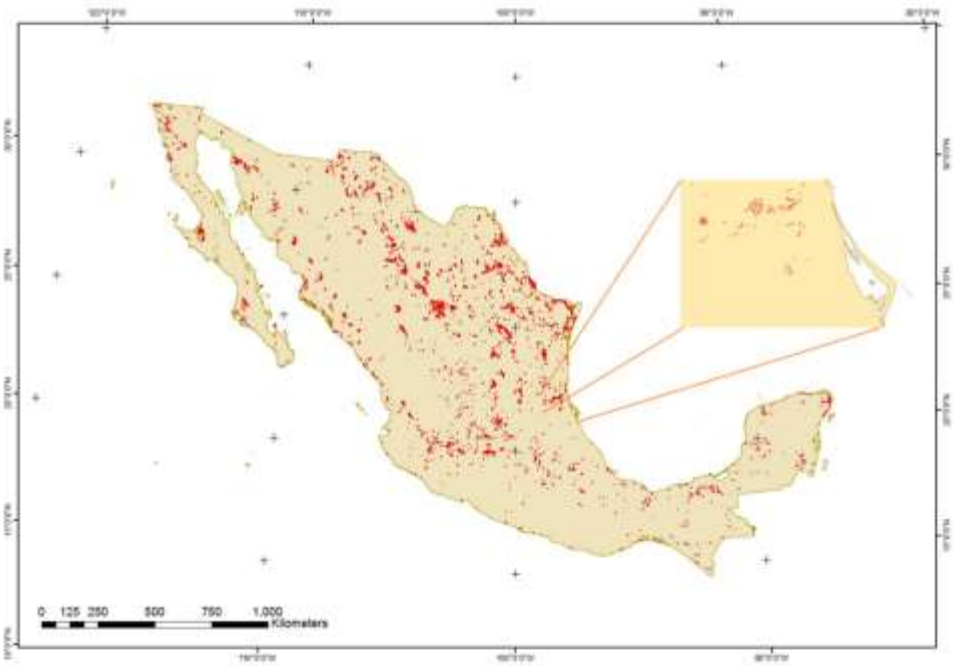

Figure 2. Final change mask with maximal potential change, red polygons represents areas detected by the algorithm based on extreme biannual differences

In order to re-digitize change polygons and assign change values to each pixel, an 11x11 grid was generated surrounding analyzed polygons; this was helpful to identify missing elements omitted by the algorithm that needed to be connected to the identified change patch. Other areas identified as change by the analyst but not detected by the algorithm were not evaluated as is shown in Figure 3. Values of 0 were assigned to no change and 1 to change.

Change assessment

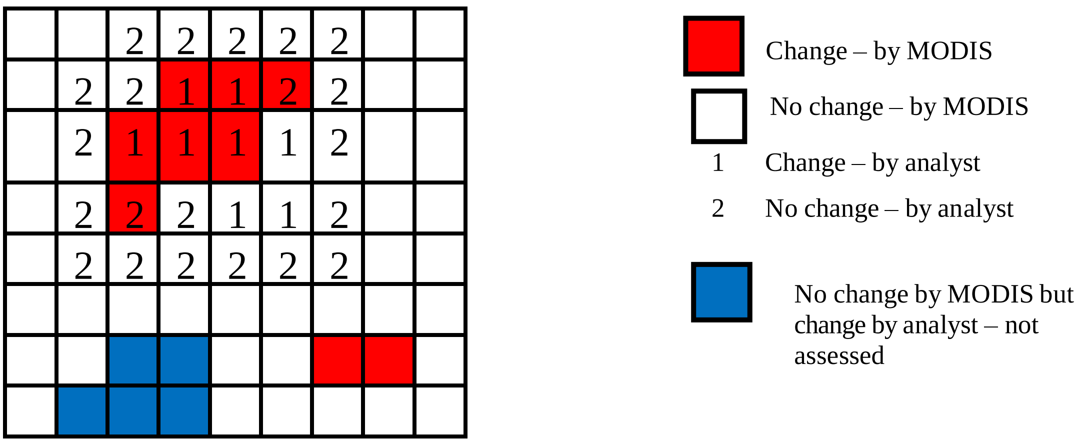

Figure 3. Criteria to evaluate change, red squares are area assessed by the algorithm; pixels with 1 are change identified by the algorithm and the analyst, those marked with 2 in red squares are areas where the algorithm detected change but analyst disagrees. Pixels marked with 2 in white squares are no change surrounding areas. Blue pixels were not evaluated

2.4 Change characterization

During the validation process, change types were assigned with six main categories as these were possible to evaluate by visual analysis. The polygons were labeled as "water/land", "vegetation loss", "burnt area", urban sprawl", "no-change" and "other", the most usual change classified as other was found on agricultural lands. It is important to mention that during the characterization process only the polygons assessed by the algorithm were evaluated.

This information helps to understand how land cover evolves in different regions according to human activities as fast population growth in big cities and natural phenomena as wild fires or atypical precipitations as well.

3. RESULTS AND DISCUSSION

3.1 Accuracy assessment

The overall agreement considering all change types as one single class except "no- change" shows 46.78%, and errors of commission and omission of 24.92% and 44.61% respectively.

The classes which perform best between reference and change mask excluding "no-change" were "urban sprawl" with commission and omission errors of 11.56% and 21.81% respectively, and "deforestation" with 11.85% and 32.78% as well. This evident agreement in these classes relies on the assumption of the extreme spectral response of the land occupied by vegetation in contrast to impervious surfaces. Remaining classes presented higher commission and omission errors as it is shown in Table 1. As it was expected, "no- change" class presented highest errors, mainly in commission (96.16%) although omission is also significant because, the analyst also assessed all areas surrounding change pixels. It has to be taken into account that our spatially-explicit assessment is much stricter than sampling- based attempts, because the area evaluated corresponds to each pixel of the change mask and connected pixels.

In addition we have to consider the difference in resolution of both sources, i.e. objects that were visually identified in Landsat cannot be detected with MODIS coarse pixels. Besides, the human eye has a different perception when detecting changes, for instance, by interpreting the surrounding area to find changes.

Table1. Percentage of commission and omission error for the six classes of change type, the corresponding area in relation to entire country is also included for each class

Change type		Commission (%)	Area (Km^2)	Omission (%)	Area (Km^2)
1	Water/Land	30.2637	887.1	40.7954	1408.6
2	Deforestation	11.8519	38	32.7784	137.8
3	Burnt area	0.92	0.625	69.9414	156.6
4	Urban sprawl	11.5645	36.3	21.8195	77.5
5	No change	96.1653	2517.2	46.7683	88.2
6	Other (Agriculture)	26.2391	193.6	39.0635	348.9

3.2 Change distribution

Observed distribution over Mexico varies for each region; most patches are concentrated over central and northern portions of the country (Figure 4) and are mainly associated to "water/land" changes and "no change" class. In the south, no large patches were detected; probably due to change areas over this region are usually small and they could not be identified by the algorithm which is based on 6.25ha pixels. Besides, when we applied the MMU to the preliminary change mask no-significant areas are not mapped.

In the Northwest, where main agricultural regions are located, there were so many polygons associated to water level changes in reservoirs which support irrigation in the coastal plain of the states of Sonora, Sinaloa and Nayarit. Also, important detected changes relate to variations in the water level were observed in the Laguna "Ojo de Liebre" in Baja California Sur due salt concentration changes. Additionally, near the city of Ensenada, Baja California, big patches of burnt area were observed. Finally for this region, "urban sprawl" was evident in Tijuana over the border between Mexico and United States, where the city has been growing towards the South and East.

The main concentration of no-change patches over northern-central part can be associated to soil humidity conditions in arid zones that represent different spectral response but which does not correspond to real land cover changes.

Water level due to flooding is also evident in Figure 4. For instance, in Mexican southeastern plain areas in Tabasco state are annually flooding as consequence of summer extreme rains associated to hurricanes in many cases. Another example is observed in US- Mexican floodways; these divert water from Rio Grande to limit flooding in the Brownsville- Matamoros urban region. The big blue polygon over this area relate to an inundation that lasted for six months in 2010 when category 2 hurricane Alex hit the coast of Tamaulipas June 30th 2010, and a few days later followed tropical depression #2. Both events caused more than 500 mm of water landfall (IBWC, 2010).

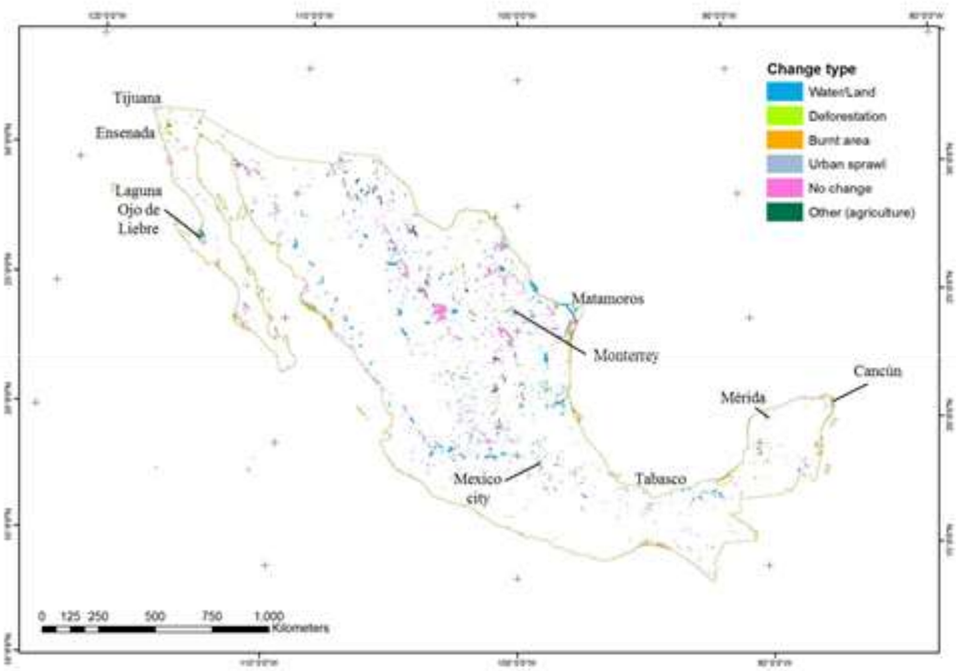

Figure 4. Change mask developed for entire Mexico, patches color indicate the type of change in accordance with ix classes established to evaluate land cover transition

Important "urban sprawl" was observed for many large cities, where migration from rural areas and fast economic growth in some cases offer conditions to urban expansion. Besides Tijuana in northwest, urban land cover changes are clearly observed around Monterrey, Nuevo León, mainly towards the North and East of the city. In Yucatan peninsula, changes were detected in urban areas of city of Mérida in the northern-central part where expansion does not seem to be directional showing patches all around the town.

Probably the best example of land cover changes due to urban expansion and detected with MODIS is the city of Cancún at the northeastern coast of the Yucatan peninsula. Until the Mexican government decided to establish a planned touristic center in late 1970's, Cancun was a small settlement of farmers of fishermen. In 2010 the population of the municipality of Benito Juárez increased to 661,176 inhabitants (INEGI, 2010). This caused an urban expansion rate of 616.4ha per year between 2005amd 2010(Veloz Avilés, 2011).

4. CONCLUSIONS

This paper presented the process for automated change detection over Mexico based on the analysis of coarse resolution MODIS images in order to generate a national change mask which can be merged with similar products of Canada and United States in the frame work of the NALCMS project. The final national products aim to present a 2010 updated version from 2005 land cover map for entire North America region.

The validation process of change mask, that instead of sampling evaluated each single pixel over the whole area, offered the chance to assign general change types according to observed features at 250m MODIS spatial resolution. Change types were classified into 6 categories established on the capability to be visually identified.

Final results allow determining commission and omission errors to entire change polygons set and being stratified by change type identified.

The spatial distribution of change patches in relation to land cover transition, allowed identifying patterns related to different regions known natural processes of the landscape, and social elements as determinant factors.

REFERENCES

Berlanga-Robles, C.A.; Ruiz-Luna, A. Land Use Mapping and Change Detection in the Coastal Zone of Northwest Mexico Using Remote Sensing Techniques. Journal of Coastal Research, v. 18, n. 3, p. 514–522, 2002.

Colditz, R.; Llamas, R.; Ressl, R. Estimating land cover changes in Mexico between 2005 and 2010 using 250m MODIS images. Journal of Selected Topics in Applied Earth Observations and Remote Sensing, 2012.

Couturier, S, Núñez, J.M, Kolb, M. Measuring Tropical Deforestation with Error Margins : A Method for REDD Monitoring in South-Eastern Mexico. In: Sudarshana, P. Tropical Forests. 2012. P. 269–296.

Feranec, J.; Jaffraini, G.; Soukup, T.; Hazeu, G. Determining changes and flows in European landscapes 1990– 2000 using CORINE land cover data. Applied Gepgraphy, v. 30, p. 19–35, 2010.

Fraser, R.H.; Olthof, I.; Pouliot, D. Monitoring land cover change and ecological integrity in Canada's national parks. Remote Sensing of Environment, v. 113, n. 7, p. 1397–1409, 2009.

Healey, S.P.; Cohen, W.B.; Zhiqiang, Y.; Krankina, O.N. Comparison of Tasseled Cap-based Landsat data structures for use in forest disturbance detection. Remote Sensing of Environment, v. 97, n. 3, p. 301–310, 2005.

Instituto Nacional de Estadística y Geografía. México: INEGI. Guía para la interpretación de cartografía, uso de suelo y vegetación Escala 1:250 000 Serie III. 2009. 74 p. Instituto Nacional de Estadística y Geografía. México: INEGI. México en Cifras, 2010. Available at: http://www.inegi.org.mx /sistemas/ mexicocifras/default.aspx.

International Boundary and Water Commission: IBWC. Rio Grande returns to normal after months of flooding, 2010.
Available at: http://www.ibwc.state.gov /Files/BM _Fall_Win_2010.pdf

Latifovic, R.; Homer, C.; Ressl, R. NORTH AMERICAN LAND CHANGE MONITORING SYSTEM. In: Giri, C. Remote Sensing of Land Use and Land Cover: Principles and Applications. CRC-Press, 2012. P. 303–324.

Manonmani, R.; Divya Suganya, G.M. Remote Sensing and GIS Application In Change Detection Study In Urban Zone Using Multi Temporal Satellite. International Journal of Geomatics and Geosciences, v. 1, n.1, p. 60–65, 2010.

Mas, J-F. Monitoring land-cover changes: a comparison of change detection techniques. International Journal of Remote Sensing, v. 20, n. 1, p. 139–152, 1999.
Mas, J-F.; Velázquez, A.; Díaz-Gallegos, J.R. Assessing land use/cover changes: a nationwide multidate spatial database for Mexico. International Journal of Applied Earth Observation and Geoinformation, v. 5, n. 4, p. 249–261, 2004.
Masek, J.G.; Huang, C.; Wolfe, R. North American forest disturbance mapped from a decadal Landsat record. Remote Sensing of Environment, v. 112, n. 6, p. 2914–2926, 2008.
Muchoney, D.M.; Haack, B.N. Change Detection for Monitoring Forest Defoliation. Photogrammetric Engineering & Remote Sensing, v. 60, n. 10, p. 1243–1251, 1994.
Pouliot, D.; Latifovic, R.; Fernandes, R.; Olthof I. Evaluation of annual forest disturbance monitoring using a static decision tree approach and 250 m MODIS data. Remote Sensing of Environment, v. 113, p. 1749–1759, 2009.
Veloz Avilés, C.A. La planeación urbana en Cancún. In: 3er Congreso Internacional de Arquitectura y Ambiente, 17., 2011.

Chlorophyll fluorescence: the signal hidden behind leaf reflectance. A new technique for the study of plant status by remote sensing

Jesús Delegido 1; Shari Van Wittenberghe 2; Carolina Tenjo 1; Jochem Verrelst 1; Luis Alonso 1; Juan Pablo Rivera 1; Neus Sabater 1; Jorge Vicent 1 and José Moreno 1

1. Department of Earth Physics and Thermodynamics. Image Processing Laboratory, Universidad de Valencia
C/ Catedrático José Beltrán, 2. 46980 Paterna (Valencia), Spain
2. University of Antwerp (UA). Dept. Bioscience Engineering. Plant Production and Stress Tolerance Research
Jesus.Delegido@uv.es

ABSTRACT

Incident solar light in terrestrial vegetation can be either reflected, absorbed or transmitted by a leaf. The absorbed light photons can be used for photosynthesis or can be dissipated into heat or emitted as fluorescence photons. In the latter case, photons are brought in an excited state of chlorophyll and emitted with a longer wavelength than light before excitation. The chlorophyll fluorescence is emitted, at leaf and canopy level, in the region 650-850 nm, with a peak located at 685-690 nm and another one at 735- 745 nm. The emitted fluoresced radiance is always super-imposed on the background reflected signal, but with a much lower intensity than the reflected radiance from the leaf, therefore it has been necessary to develop techniques that allow separating both signals from remotely sensed radiance. This fluorescence signal is instantly related to the functional status of the photosynthetic apparatus. Monitoring of this excess energy dissipation pathway provides a tool for detecting early stress symptoms of vegetation - that is, before damage is irreversible. This responsive feature of fluorescence also supports practical applications such as agronomic crop improvement and forest vegetation assessment in the face of climatic instability.
The growing interest on the potential of measuring chlorophyll fluorescence from remote sensing on a global scale recently led to the initiation of the Fluorescence Explorer (FLEX) mission. FLEX, currently under development phase A/B1 of the 8th European Space Agency (ESA) Earth Explorer Program, aims to be the first space mission primary dedicated to the estimation of chlorophyll fluorescence at a global scale. Our group is involved in various FLEX-related research activities and a brief overview of their latest status will be presented.

Keywords: FLEX, Fluorescence, Photosynthesis, Chlorophyll

1. FLUORESCENCE IN PHOTOSYNTHESIS

Photosynthesis is the plant process that synthesizes organic compounds from inorganic substances in the presence of sunlight. The most important step, chemically, in photosynthesis is the conversion of carbon dioxide and water into carbohydrates and oxygen. The first photosynthesis part is an energy conservation phase that includes the formation of an electron transfer redox chain and the consequent generation of a protons concentration gradient. Thylakoids (sheet structures inside chloroplasts) contain protein complexes that perform the management of electrons and protons necessary for energy conversion. The protein complexes in thylakoid included are four; two of them are photosystems, namely, systems capable of absorbing and transforming energy photon in redox electrochemical energy. They are called photosystem I (PSI) and photosystem II (PSII). Each one has a different spectral absorption shape of chlorophyll- *a* in the reaction centre. The chlorophyll of photosystem I, called P700, absorbs light at infrared wavelengths (735-745 nm) and the PSII chlorophyll called P680, absorbs at red wavelengths (650- 850 nm) (Figure 1a). The third complex is a connector between the two systems, called b_6f cytochrome complex. Finally there is a fourth protein complex not involved in the transfer of electrons, but using the proton gradient generated the other complex through the thylakoid to synthesize. When the chlorophyll-*a* molecule present in PSI and PSII is irradiated with electromagnetic radiation, is able to absorb a certain quantity of the same energy corresponding to a photon with the same energy quantity that is necessary to excite an electron from the molecule of chlorophyll-*a* and cause the jump of the electron to a higher energy orbital, leaving the chlorophyll-*a* molecule in an excited state (Figure 1b). The chlorophyll-*a* molecule is not stable in that excited state and must return to its fundamental energy state, and therefore, must transfer the excitation energy. There are three ways in which the electron recovers its fundamental state: 1. Photochemical processes, photosynthetic activity, included CO_2 assimilation, consuming the ATP and NADPH generated in the initial phase of photosynthesis. 2. No photochemical processes, mainly the thermal dissipation (no radiant) of the excitation energy. 3. Light re-emission (fluorescence (F)). As seen, the F signal is related to photosynthesis, allowing a direct estimate of the actual photosynthetic activity of the vegetation. In fact, F emission occurs in competence with photosynthesis and heat dissipation (Figure 1c). Under stress conditions, plants show a decrease of photosynthetic activity due to a change in the distribution of the energy absorbed in the three scope processes. However, F measurement is difficult because it represents a small amount of the total radiance measured by a sensor to be masked by the light reflected by the plant itself (Figure 2) (Gomez-Chova et al., 2006).

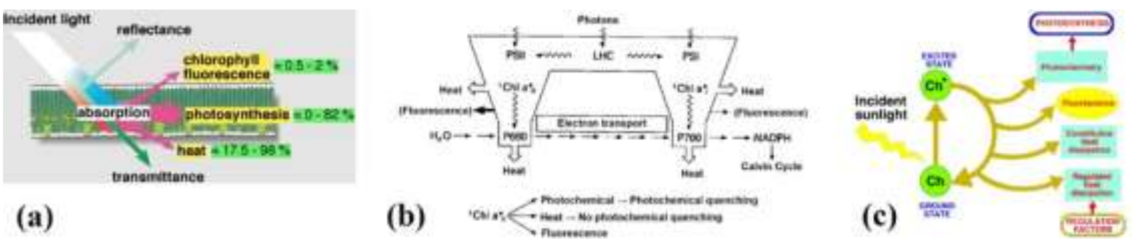

Figure 1. (a) The fate of light within leaves (ESA, 2008). (b) The different processes of light energy dissipation in photosynthesis (Cendrero, 2010). (c) Scheme of light-energy capture by chorophyll molecules and the different dissipation mechanisms used to return to the ground-state energy-level (ESA, 2008)

The PSI and PSII are responsible for the F emission and as each of them has one shape of chlorophyll-*a* in the reaction centre spectrally different, therefore, the light re-emission is spectrally different. P700 absorbs light at infrared wavelengths and therefore is responsible for the F emission peak in the infrared (F740) and P680 absorbs at red wavelengths and therefore is responsible for the fluorescence emission in the red peak (F690) (Figure 2a).

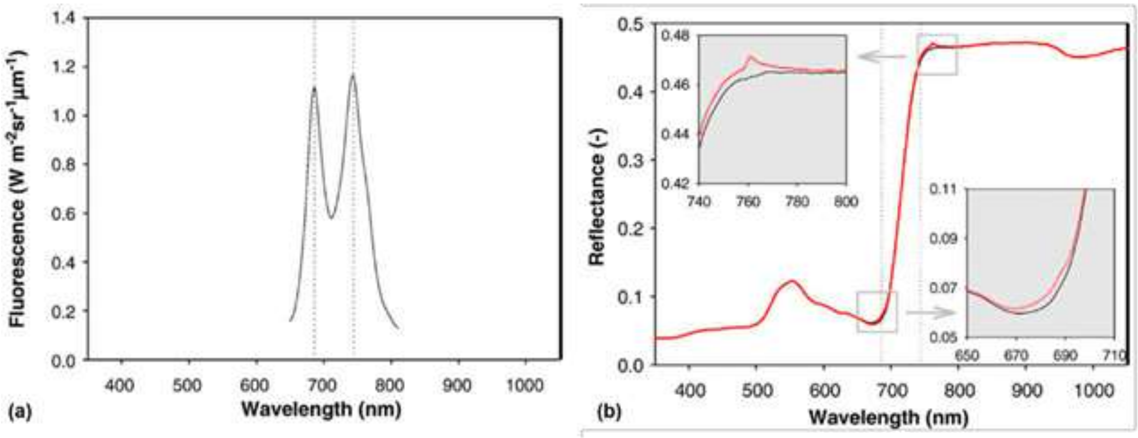

Figure 2. Solar-induced Chl fluorescence and reflectance spectra of a sugar beet leaf. (a): F spectrum in the region between 650 and 800 nm. (b): The actual reflectance (black curve) was computed as the ratio of the reflected and incident fluxes; the apparent reflectance (red curve) was computed as the ratio of the total upwelling flux (reflection plus F) and the incident flux. The difference between the two quantities is highlighted in the grey boxes, showing the responses surrounding the F emission maxima (vertical dotted lines) (Meroni et al., 2009)

Although fluorescence, photosynthesis and non-photochemical protection are closely connected, the translation of fluorescence data to photosynthesis is not trivial. In fact, while under low light unstressed conditions (no non-photochemical protection mechanisms activated) a negative correlation exists between fluorescence and photochemistry, most studies have observed that in the presence of plant stress and high light conditions, fluorescence declines with photosynthesis as a result of protective mechanisms which take place in the leaf to prevent damage caused by harmful radicals formed in such stress conditions (Van der Tol et al., 2009).

2. FLUORESCENCE AND REMOTE SENSING

The study of solar induced fluorescence (SIF) (also known as 'passive' fluorescence) is one important research objective for space-based platforms. In some ways it is a more mysterious phenomenon than actively-induced fluorescence because a given signal level cannot be unambiguously interpreted without consideration of aspects such as atmospheric and environmental information, or the pattern of SIF behavior over time (necessitating repeat measurements). SIF typically has been studied with respect to the changes in the ratio of the Red:NIR peaks that occur with physiological fluctuations. The ratio has been shown to be responsive to chlorophyll content, decreasing with increasing chlorophyll as a result of greater re- absorption of the red F in the leaf. SIF also responds to photosynthetic fluctuations independently of chlorophyll content (Lichtenthaler & Rinderle, 1988). Comparisons between active and passive F measurements, photosynthesis yield, and photosynthesis rate have also been made (Carter et al., 1990; Moya et al., 2004; Meroni and Colombo, 2006). SIF has been successfully correlated to photosynthesis at the leaf scale, and in a preliminary way at the canopy scale. Simple ratios of the two peaks or other features such as the numerical value of the integral between peaks normalized over a parameter such as absorbed or incident PAR are examples of how SIF information may be considered for use in characterizing photosynthetic performance and resilience.

The capacity to observe SIF presents a complete novel option for space-based remote sensing, by extracting information on the real-time workings of the photosynthetic machinery of plant canopies. Because the production of CF is related to the function of the two photosystems active during photosynthetic initiation in green plants, it provides an actual glimpse into the dynamics of the photosynthetic process. As a photosynthesis indicator, F may be envisaged for use in:

- tracking vegetation responses to stress, including resilience and recovery from natural or human-induced perturbations
- quantifying photosynthetic efficiency, which can serve as a proxy for light use efficiency in gross primary productivity (GPP) and global carbon models
- investigating implications for photosynthetic rate, and possibly even more directly helping to quantify GPP Plant F under solar illumination adds a weak signal to reflected solar radiation. If both fluorescence emission and surface reflectance are assumed to follow Lambert's law, the radiance upwelling from vegetation (L) at ground level is therefore composed of two coupled contributions, one reflected (r E/π) and the other emitted (F) (Meroni et al., 2009):

$$L(\lambda) = \frac{r(\lambda)E(\lambda)}{\pi} + F(\lambda) \quad \left[\mathrm{W\ m^{-2}\ sr^{-1} \mu m^{-1}}\right] \tag{1}$$

where λ is wavelength, r is reflectance (free of the emission component), and E is total irradiance incident on the target. Even though F contributes to the signal detected by a remote sensor, its magnitude is small (1–5% of the reflected radiation in the near infrared) thus making the decoupling of the two contributions difficult. Zarco-Tejada et al. (2000) first recognized the effect of F on reflectance and demonstrated that it is possible to detect the F signal using reflectance measurements. In fact, the reflectance factor usually computed by the RS community as the ratio between upwelling and incident fluxes is indeed polluted by the F contribution (Meroni et al., 2009):

$$r^*(\lambda) = \frac{\pi L(\lambda)}{E(\lambda)} = r(\lambda) + \frac{\pi F(\lambda)}{E(\lambda)} \quad [-]. \tag{2}$$

This quantity, referred here as apparent reflectance, r*, differs from the pure reflectance (r) as indicated by the right hand side of Eq. (2) and as shown in Figure 2b.

The F signal is comparably stronger and can be detected passively in narrow dark lines of the solar and atmospheric spectrum in which irradiance is strongly reduced (the so-called Fraunhofer lines). In the visible and near-infrared, the solar spectrum at ground level exhibits three main “Fraunhofer” features which have been exploited for F estimation: Hα due to hydrogen (H) absorption in the solar atmosphere (centered at 656.4 nm) and two telluric oxygen (O2) absorption bands in the Earth atmosphere, O2-B (687.0 nm) and O2-A (760.4 nm). The incident at-surface irradiance at different spectral resolutions (0.005, 0.1 and 1.0 nm Full Width at Half Maximum, FWHM) and at the spectral regions around these three absorption features is shown in Figure 3. Irradiance data were simulated by means of the Matrix Operator Model (MOMO) (Fell & Fischer, 2001). Among other inputs, the sun zenith angle was set to 30°, with a mid-latitude summer atmosphere, the surface at sea level, and the aerosol optical thickness at 550 nm equal to 0.2. Resampling to the different spectral resolutions was performed assuming Gaussian-like spectral response functions with the given FWHM (Meroni et al., 2009).

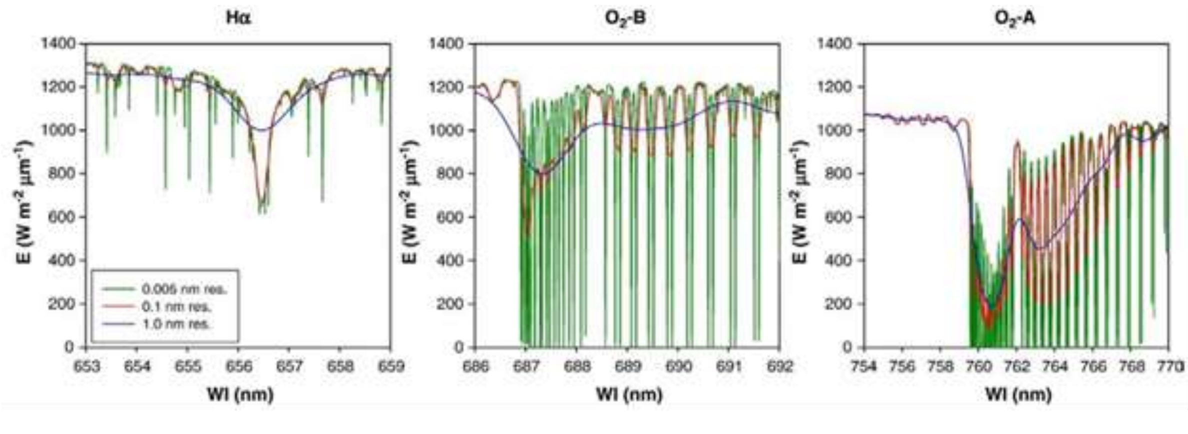

Figure 3. Incident irradiance (E) at ground level at the three absortion lines normally used for F retrieval and at three different spectral resolutions (Meroni et al., 2009)

Recently, alternative retrieval algorithms based on the spectral fitting of hyperspectral radiance observations, Spectral Fitting Methods (SFMs), have been proposed. FLD and SFMs were used to estimate F starting from Top Of Canopy (TOC) fluxes at very high spectral resolution (0.12 nm) and sampling interval (0.1 nm), exploiting the O2-B (687.0 nm) and O2-A (760.6 nm) atmospheric oxygen absorption bands overlapping the fluorescence emissions at the red and far-red spectral window, resulting that violation of FLD assumptions results in a positive bias in F estimation at both oxygen absorption bands that cannot be avoided even at the high spectral resolution considered (Meroni et al., 2010).

3. PAST PROJECTS

Projects carried out over the past decade have served as valuable proof-of-concept studies for remote measurement of SIF:

- SIFLEX (Solar Induced Fluorescence Experiment, executed over Finland in 2003) demonstrated that SIF was discernible even in boreal conditions using tower-based or airborne instrumentation.
- SEN2FLEX (Sentinel-2 and FLEX Experiment in 2005) used a new airborne instrument AirFLEX and the CASI (Compact Airborne Spectrographic Imager) to reveal that the fluorescence signal contains information not apparent in classical remote-sensing observation.
- CEFLES 2 (CarboEurope, FLEX and Sentinel-2, carried out in Southern France in 2007) showed that canopy fluorescence is indeed closely correlated with ecosystem carbon uptake and that fluorescence data improve diurnal model predictions of GPP. On the regional scale, the fluorescence signal could be correlated to regional airborne measurements of carbon fluxes.
- FluorMOD project (Miller et al. 2005), was a seminal work funded by ESA, which undertook to model leaf and canopy fluorescence. An integrated model was developed, comprising the sub-models FluorMODleaf and FluorSAIL. The focus was to create a model for unstressed vegetation, though it did accommodate diurnal downregulation. The decision to emphasize fluorescence under benign conditions permitted understanding what ‘normal’ fluorescence behavior looks like, so that one application of the FluorMOD results could be to help identify the existence of stress based on the deviation of measured results acquired from space against an unstressed ‘baseline’ or ‘control’. FluorMOD predicted that SIF might, indeed, be measurable from a space-based platform. Developments linked to the FluorMOD work include an improved leaf emission spectrum taking into account emission of the two photosystems involved in the initial states of photosynthesis (Pedrós et al., 2008), and a further elucidation of FluorMODleaf that incorporated re-absorption of emitted fluorescence (Pedrós et al., 2010). This model simulates apparent spectral fluorescence yield of a fresh leaf between 640 and 840 nm for any excitation light of the visible spectrum.
- In other recent work (separate from FluorMOD), a computational procedure was developed to resolve the respective contributions of PSI and PSII to the leaf chlorophyll fluorescence emission spectra at room temperature (Palombi et al., 2011). The approach used Principal Component Analysis of fluorescence emission in the O-I kinetic induction phase. A single- band spectrum for fluorescence emission peaked at about 735 nm for PSI, and a 2-band spectrum with maxima at 685 and 740 nm for PSII was identified. A linear combination of only these two spectral shapes yielded a good fit for any measured emission spectrum of the leaf under investigation (*Ficus benjamina*) and may be useful for discerning the fluorescence emission contributions of the photosystems under different conditions. Thus, the dynamics of energy distribution between the two photosystems may be monitored at physiological (~room) temperatures rather than having to use -196°C to study PSI emission as has been done in the past. Separation of the PSI and PSII emission components can improve our understanding of the changes in fluorescence signal induced by environmental factors or stress conditions, and may be helpful for interpreting remotely captured fluorescence.

4. FLEX MISSION

FLEX will be the first space mission designed to optimize remote observation of the chlorophyll fluorescence in terrestrial vegetation. The ESA mission will undertake to provide global maps of vegetation-fluorescence emissions. These might then be converted into photosynthetic efficiency for use in global monitoring of health and stress resilience. The

Photosynthesis Study will provide useful recommendations for generation of spatial-temporal maps of vegetation health and stress status in near real-time.

FLEX will take advantage of additional measurements provided by the Ocean and Land Colour Instrument (OLCI) and the Sea and Land Surface Temperature radiometer (SLST) onboard Sentinel-3. The combined information is critical to resolve the disagreements between different land models that attempt to simulate future atmospheric CO_2 concentrations through interactive terrestrial carbon balances.

The objective is a global coverage mission, monitoring vegetation photosynthesis along the seasonal cycles and the activation/deactivation of the photosynthetic mechanisms where photochemistry is adjusted to a lesser or greater level of activity. Global coverage should be achieved for all land surfaces between -56° and +75° latitude including major islands.

FLEX will be a satellite flying in tandem with Sentinel-3. Observations of FLEX and S-3 will be acquired within 6 to 15 s from each other. Payload is the FLuORescence Imaging Spectrometer (FLORIS) measuring fluorescence in O2-A and O2-B bands plus reflectance over red-edge and Photochemical Reflectance Index (PRI) spectral ranges. FLORIS operates in pushbroom mode with a swath of 100 to 150 km (contained within one of the S-3 OLCI camera swath) and a pixel size of 0.3 x 0.3 km². Data in four spectral bands: O2-A (750-777 nm); O2-B (660-714 nm); red edge (714-750 nm); PRI (520-660 nm) with sampling of 0,1 nm in oxygen bands and 0,5 to 2 nm in red edge and PRI bands calibration relies on both cross-calibration with the equivalent bands of OLCI and dedicated devices. FLEX and S-3 images co-registered by on-ground processing through correlation algorithms. Vega launcher as baseline and mission duration of nominally 3,5 years (to cover at least 3 full vegetation growth cycles) with goal of 5 years.

The optimal spatial resolution for observing land targets and monitor surface processes is difficult to define, since almost all spatial scales are important. Land-atmosphere interactions can hardly be modeled in high detail for large areas and in most cases the surface—atmosphere coupling is represented at reduced spatial resolution. In the particular case of carbon exchanges between surface and atmosphere, the combination of requirements provides an optimum spatial resolution in the range of 100-300 m, which is detailed enough to identify vegetated patches while resolving interactions at scales comparable to typical heights of the atmospheric boundary layer. Here a resolution of 100—300 m would be reasonable as well and in line with other data sources and modeling efforts.

5. BIOHYPE PROJECT

Biomonitoring of natural vegetation allows the acquisition of well-defined samples at anaffordable cost and allows determining air pollution at different time-scales. It reflects longer-term changes of environmental quality, because plant leaves accumulate pollution over months, or even years for evergreen species. In the BIOHYPE project, biomonitoring is organized at three tree structural levels: (i) the sub-leaf level, (ii) the leaf level and (iii) the canopy level. An airborne hyperspectral based biomonitoring is applied to cover the goals at canopy scale. The overall research goal is to develop, test and validate a passive biomonitoring methodology based on hyperspectral observations and based on a field experimental approach which lapses over several spatial scales as well as over several tree structural and temporal levels, depending on the parameter considered. One of main goals of the project is the investigation at sub-leaf, leaf and canopy level of the spatial distribution of chlorophyll fluorescence. These objectives will be fulfilled by two broad field and flight campaigns in two cities of two different climatic zones: Ghent (Belgium) and Valencia (Spain). The scientific outcome of the project will foster thorough knowledge of the correlation between tree characteristics at the sub-leaf, leaf and canopy levels and air pollution. Moreover, a more profound knowledge can be acquired concerning the correlation between the different tree level structural characteristics, and quite specifically the relevance and biomonitoring potential of airborne hyperspectral, as well as chlorophyll fluorescence data. Up and downward fluorescence yield are, to some extent, linearly related to each other, but depending on the leaf anatomy and chlorophyll content, the ratio or fitting can differ. It is known that chlorophyll is one of the drivers of the first fluorescence peak, hereby reflecting the activity of photosystem II (Figure 4) (SR/00/131, 2012). Results also show that SIF acts as a more sensitive indicator of (traffic) pollution stress compared to more static biochemical variables such as chlorophyll content (Van Wittenberghe et al., submitted).

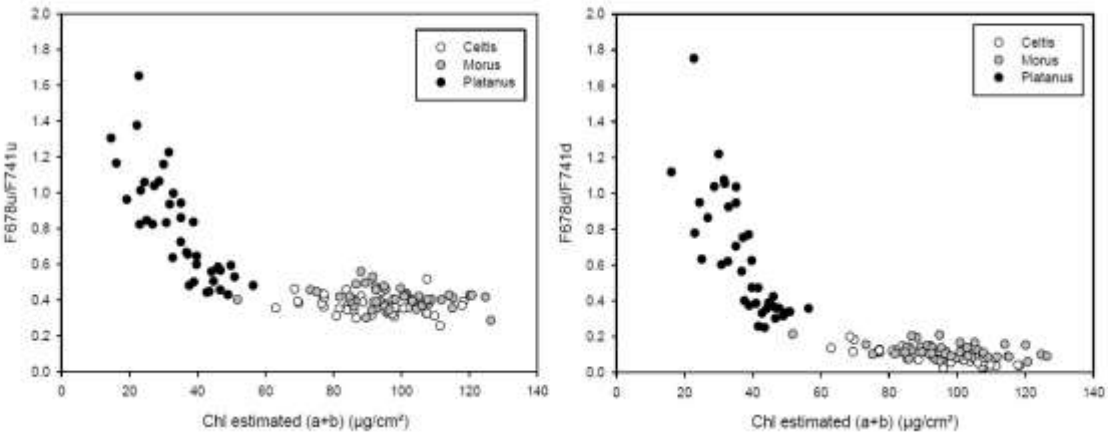

Figure 4. The fluorescence ratio F678/F741 upward and downward versus the estimated chlorophyll content

6. EXAMPLE OF ESTIMATION OF SOLAR-INDUCED VEGETATION FLUORESCENCE FROM SPACE MEASUREMENTS

In this example, a methodology for the estimation of solar-induced chlorophyll fluorescence from spaceborne and airborne sensors is presented. The fluorescence signal is included in an atmospheric radiative transfer scheme so that chlorophyll fluorescence and surface reflectance are retrieved consistently from the measured at-sensor radiance. This methodology is tested on images acquired by the Medium Resolution Imaging Spectrometer (MERIS) on board the ENVIronmental SATellite (ENVISAT) taking advantage of its good characterization of the O2-A absorption band. Validation of MERIS-derived fluorescence is carried out by applying the method to data acquired by the Compact Airborne Spectrographic Imager (CASI-1500) sensor concurrently to MERIS acquisitions (Figure 5). CASI-derived fluorescence is in turn compared with ground-based fluorescence measurements, a correlation coefficient R^2 of 0.85 being obtained (Guanter et al., 2007).

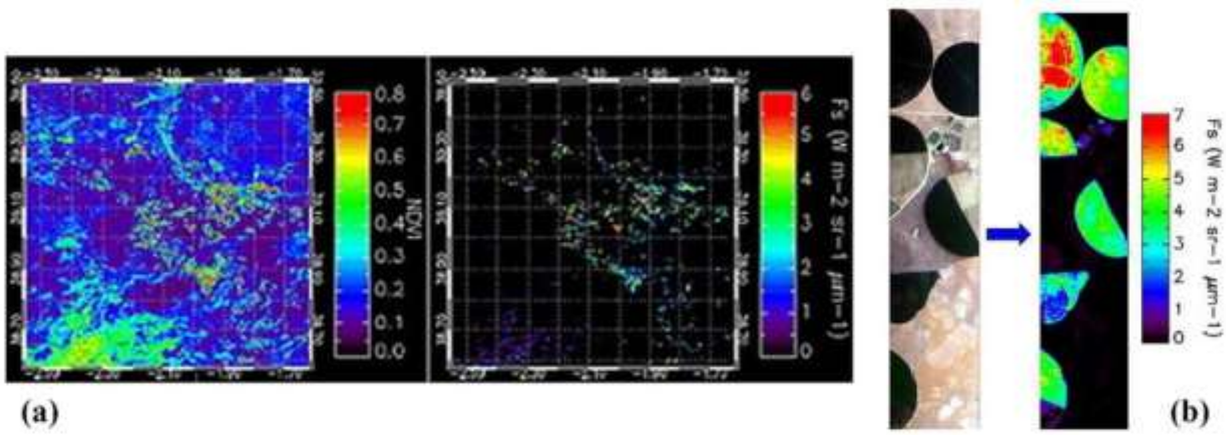

Figure 5. Fluorescence maps obtained from a MERIS (a) and CASI (b) images (Guanter et al., 2007)

REFERENCES

Carter, G., Theisen, A., & Mitchell, R. Chlorophyll fluorescence measured using the Fraunhofer line-depth principle and relationship to photosynthetic rate in the field. Plant, Cell & Environment, v. 13, p.79-83, 1990.

Cendrero, P. Estudio comparativo de métodos de estimación de fluorescencia de la vegetación: impacto de la resolución espectral. Valencia: Universidad de Valencia. 2010.

ESA. FLEX - Fluorescence Explorer. The Netherlands. 2008.

Fell, F., & Fischer, J. Numerical simulation of the light field in the atmosphere–ocean system using the matrix- operator method. Journal of Quantitative Spectroscopy and Radiative Transfer, n. 69, p. 351–388, 2001.

GomezChova, L., Alonso-Chorda, L., Amoros Lopez, J., Vila Frances, J., del ValleTascon, S., Calpe, J. M. Solar induced fluorescence measurements using a field spectroradiometer. Earth Observation for Vegetation Monitoring and Water Management, 2005.

Guanter, L., Alonso, L., Gomez-Chova, L., Amorós-López, J., Vila, J., & Moreno, J. Estimation of solar-induced vegetation fluorescence from space measurements. Geophysical Research Letters, n. 34(08401), 2007.

Lichtenthaler, H., Rinderle, U. The role of chlorophyll fluorescence in the detection of stress conditions in plants. CRC Crit Rev Anal Chem, n. 19, p. 29-85, 1988.

Meroni, M., & Colombo, R. Leaf level detection of solar induced chlorophyll fluorescence by means of a subnanometer resolution spectroradiometer. Remote Sensing of Environment, n. 103, p. 438-448, 2006.

Meroni, M., Busetto, L., Colombo, R., Guanter, L., Moreno, J., Verhoef, W. Performance of Spectral Fitting Methods for vegetation fluorescence. Remote Sensing of Environment, n. 114, p. 363–374, 2010.

Meroni, M., Rossini, M., Guanter, L., Alonso, L., Rascher, U., Colombo, R., Moreno, J. Remote sensing of solar-induced chlorophyll fluorescence: Review of methods and applications. Remote Sensing of Environment, n. 113, p. 2037–2051, 2009.

Miller, J., Berger, M., Goulas, Y., Jacquemoud, S., Louis, J., Mohammed, G., Moise, N., Moreno, J., Moya, I., Pedrós, R., Verhoef, W., Zarco-Tejada, P. Development of a Vegetation Fluorescence Canopy Model. European Space Agency. ESTEC Contract No. 16365/02/NL/FF, Final, 2005.

Moya, I., Camenen, L., Evain, S., Goulas, Y., Cerovic, Z., G., L., Flexas, J., Ounis, A. A new instrument for passive remote sensing 1. Measurements of sunlight-induced chlorophyll fluorescence. Remote Sensing of Environment, v. 91 n. 2, p. 186-197, 2004.

Palombi, L., Cecchi, G., Lognoli, D., Raimondi, V., Toci, G., Agati, G. A retrieval algorithm to evaluate the Photosystem I and Photosystem II spectral contributions to leaf chlorophyll fluorescence at physiological temperatures. Photosynthesis Research, n. 108, p. 225-239, 2011.

Pedró, R., Moya, I., Goulas, Y., Jacquemoud, S. Chlorophyll fluorescence emission spectrum inside a leaf. Photochem Photobiol Sci, n. 7, p. 498-502, 2008.

Pedrós, R., Goulas, Y., Jacquemoud, S., Louis, J., Moya, I. FluorMODleaf: A new leaf fluorescence emission model based on the PROSPECT model. Remote Sensing of Environment, n. 114, p. 155-167, 2010.

SR/00/131, BIOHYPE: BIOmonitoring of urban habitat quality with airborne HYPErspectral observations. C. N. (Ed.). Research programme for Earth observation stereo II, 2012.

Van der Tol, C., Verhoef, W., Rosema, A. A model for chlorophyll fluorescence and photosynthesis at leaf scale. Agricultural and Forest Meteorology, v. 149, n. 1, p. 96-105, 2009.

Van Wittenberghe, S., Alonso, L., Verrelst, J., Hermans, I., Delegido, J., Veroustraete, F., Valcke, R., Moreno, J., Samson, R. submitted to Environmental Pollution, 2013.

Zarco-Tejada, P. J., Miller, J. R., Mohammed, G. H., Noland, T. L. Chlorophyll fluorescence effects on vegetation apparent reflectance: I. Leaf-level measurements and model simulation. Remote Sensing of Environment.

Comparación de valores NDVI de LANDSAT 5 TM y MODIS en lotes agrícolas de Entre Ríos y campañas con precipitaciones contrastantes

Nicolás Vaiman 1; Armando Brizuela 1-2 y César Aguirre 1-2

1. Facultad de Ciencias Agropecuarias, UNER, Oro Verde, Argentina
2. Centro de Investigaciones Científicas y Transferencia de Tecnología a la Producción, CONICET

Diamante, Entre Ríos, Argentina
nicolasvaiman@hotmail.com

RESUMEN

En este trabajo se compararon valores de NDVI de Landsat 5 TM y de MODIS en dos campañas agrícolas contrastantes en lo referido a las precipitaciones y se determinó la correlación entre datos de ambos sensores. El área de estudio se ubica al Oeste de Entre Ríos donde se identificaron, en cada campaña, diez lotes de maíz, de soja, de trigo y de soja de segunda. Los datos de precipitaciones pertenecen a siete estaciones meteorológicas de la Dirección de Hidráulica de Entre Ríos. Se realizó un análisis estadístico de los valores de NDVI teniendo en cuenta los períodos críticos durante los cuales se determina el rendimiento. En 2008 las precipitaciones fueron 52% menores al promedio histórico, en cambio, en 2009 resultaron un 20% mayor a dicho promedio. Los valores de NDVI presentaron diferencias significativas entre campañas, y en algunos casos -maíz, soja de segunda- según la fuente del NDVI, Landsat o MODIS. El máximo NDVI de Landsat se halló en maíz (0,89) y el mínimo en trigo (0,47); en MODIS, el máximo NDVI se observó en soja y soja de segunda (0,84) y el mínimo en trigo (0,46). Los valores máximos corresponden a la campaña 2009/10 y los mínimos a la campaña 2008/09. Los coeficientes de determinación hallados entre datos de Landsat y de MODIS resultaron elevados, con un mínimo R^2 de 0,73 y un máximo de 0,92 en soja. Esto determina que ambos sensores fueron capaces de detectar las diferencias de vigor de los cultivos en ambas campañas.

Palabras clave: NDVI, Landsat, MODIS, cultivos, sequía.

ABSTRACT

In this study we compare Landsat 5 TM and MODIS NDVI values in two agricultural years with contrasting precipitation amounts, and correlation between both sensors data was determined. The study area is located in western Entre Ríos, and we worked with ten fields of each crop under study (corn, soybean, wheat and second-crop soybean) in both years. Precipitation data came from seven meteorological stations that belongs to the Dirección de Hidráulica de Entre Ríos. We performed a statistic analysis of NDVI values considering critic periods for yield determination. In 2008, precipitations were 52% less than historical average, but in 2009 precipitations were 20% higher. NDVI values were significantly different comparing between years, and in some cases -corn and second-crop soybean- comparing between sources of NDVI, Landsat or MODIS. The highest Landsat NDVI value was observed in corn (0.89) and the lowest one in wheat (0.47); the highest MODIS NDVI value was found in soybean and in second-crop soybean (0.84) and the lowest one in wheat (0.46). Maximum values belong to 2009/10 and minimum values belong to 2008/09. High determination coefficients were found between Landsat and MODIS data, with the lowest R^2 of 0.73 in corn and the highest $R^2$of 0.92 in soybean. This determines that both sensors were able to detect crop vigor differences between years.

Keywords: NDVI, Landsat, MODIS, crops, drought.

INTRODUCCIÓN

La diferencia normalizada de energía reflejada en las regiones del infrarrojo y del rojo del espectro electromagnético ha sido el centro de atención para el desarrollo de índices cuantitativos con el objetivo de estimar la condición de la vegetación a través de imágenes de sensores remotos (Thiam y Eastman, 2006). Cuando la vegetación comienza a sufrir un estrés, esta condición puede ser revelada por cálculos de NDVI, debido a que el color verde típico de una vegetación sana y vigorosa comienza a tomar tintes marrones lo que aumenta la reflectancia en esas longitudes de onda. La vegetación estresada presenta una mayor reflectividad en la región del visible (400-700 nm) en comparación con la vegetación sana. A su vez, este comportamiento se invierte en la región del irc (750-1200 nm) y esta diferencia se puede utilizar para caracterizar el estado de los cultivos (Kyllo, 2003).

La sequía es una adversidad recurrente en la agronomía, afectando las cosechas agrícolas y la producción ganadera en distinto grado de intensidad. Los medios tradicionales que se utilizan para identificar, caracterizar o evaluar la sequía, se fundamentan en la aplicación de información meteorológica, expresando el desequilibrio hídrico a partir de indicadores elaborados con variables atmosféricas u obtenidos por medio de procedimientos de balance hidrológico.

La precisión de procedimientos convencionales utilizados para evaluar la sequía decrece a medida que la proyección se aparta del lugar de origen de la información primitiva, lo que para las variables relacionadas con la precipitación torna el resultado incierto o tentativo a escasos kilómetros de distancia, incluso en regiones llanas (Hubbard, 1994; Rotondo y Seiler, 2001).

Las mediciones satelitales para el seguimiento de la vegetación presentan, en cambio, las siguientes ventajas: son realizadas por un único observador, ofrecen una visión sinóptica, en muchos casos su uso tiene un costo nulo y alcanza una visión repetitiva de aproximadamente toda la superficie de la Tierra (Johnson et al., 1993), lo que constituye un recurso más idóneo para el seguimiento de la vegetación que los datos meteorológicos.

Los trabajos de Ji y Peters (2003) utilizando series de tiempo de NDVI y su asociación con el Índice Estandarizado de Precipitación (Mc Kee et al., 1995) para detectar las regiones afectadas por sequías, y el de Zang et al. (2005) empleando el producto MODIS NDVI y MODIS LAI (índice de área foliar) para elaborar el índice de impacto de la variabilidad climática (CVII, por sus siglas en inglés), que cuantifica el porcentaje de la producción anual, tanto ganado como perdido debido a la variabilidad climática, dan cuenta de la importancia de la teledetección en el monitoreo de sequías y tratan de cuantificar las pérdidas de producción agrícola causadas por ellas. También se ha simulado la condición y el rendimiento de cultivos utilizando datos de Landsat y MODIS (Doraiswamy et al., 2004).

A su vez, el análisis multitemporal del NDVI es de gran importancia para determinar adelantos o retrasos en el desarrollo y la senescencia foliar y también ha sido utilizado para estimar distintos parámetros de los cultivos y separar aquellos con patrones fenológicos distintos (Fischer, 1994).

El objetivo de este trabajo es analizar y comparar datos provenientes de los satélites Landsat 5 TM y MODIS en dos campañas agrícolas contrastantes en lo referido a las precipitaciones y determinar la correlación entre datos de NDVI de ambos sensores.

MATERIALES Y MÉTODOS

El área de estudio se encuentra delimitada por el paralelo 31º41´33´´ S en el Norte y el paralelo 32º11´58´´ S en el Sur, y desde el meridiano 60º13´58´´ W al Este hasta el meridiano 60º41´12´´ W al Oeste. Estas coordenadas corresponden a la región centro Oeste de la provincia de Entre Ríos, Argentina (Figura 1).

Figura 1. Localización del área de estudio

Para caracterizar las precipitaciones de la provincia de Entre Ríos durante las campañas agrícolas evaluadas (2008/09 y 2009/10), se utilizó el registro de datos de siete estaciones meteorológicas automáticas (EMA) de la Dirección de Hidráulica de Entre Ríos: Gualeguaychú, Villaguay, Basavilbaso, La Paz, Paraná, Puerto Yeruá y Diamante (http://www.hidraulica.gov.ar/precipitacionesHistorico.php).

Se localizaron mediante GPS diez lotes de cada cultivo evaluado en ambas campañas (trigo, maíz, soja y soja de segunda) y en cada lote se confeccionaron 3 áreas de muestreo, cada una de 6x6 píxeles en las imágenes Landsat 5 TM (equivalente a 3,24 ha), totalizando 30 muestras por cultivo. En estos mismos lugares se registró el valor de NDVI proveniente de un píxel en las imágenes MODIS (equivalente a 6,25 ha). En la figura 2 se puede apreciar un sector del área de estudio.

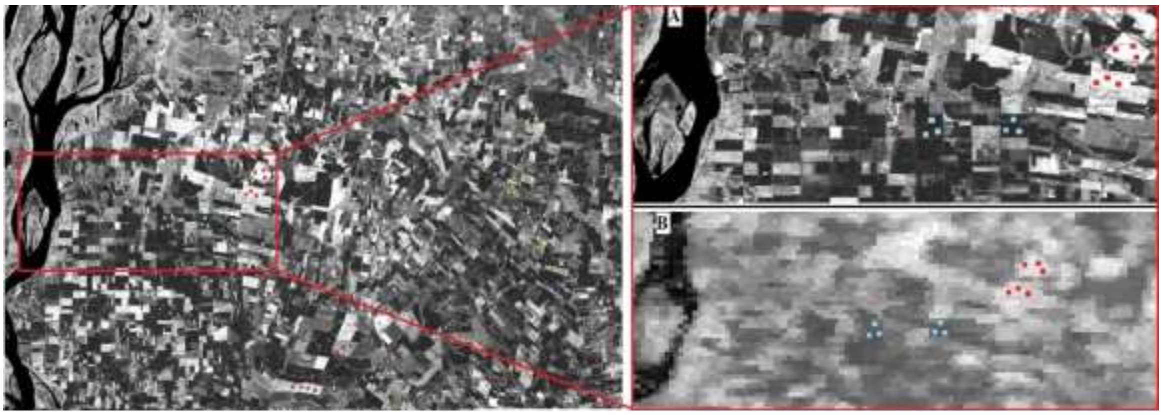

Figura 2. Zona del área de estudio en donde se pueden apreciar algunas áreas de muestreo en una imagen A) Landsat 5 TM y B) MODIS

Se trabajó con imágenes Landsat 5 TM pertenecientes a las órbitas 226 y 227, fila 82, y con el producto MODIS/Terra MOD13Q1, que ofrece información de índices de vegetación integrando 16 días de datos.

Para los meses en que normalmente ocurren los períodos críticos para la determinación del rendimiento de los cultivos (Tabla 1), se procedió a realizar un análisis estadístico para detectar diferencias entre los valores de NDVI de cada campaña y para comparar entre satélites ya que en los últimos estados vegetativos hasta inicio del llenado de granos, las imágenes satelitales describen mejor el rendimiento esperado en varios cultivos (Yang et al., 2001).

Tabla 1. Fechas de las imágenes utilizadas para comparar valores de NDVI entre campañas

	Imágenes Landsat 5 TM		Imágenes MODIS	
Cultivo	2008/09	2009/10	2008/2009	2009/10
Trigo	20-sep-08	14-sep-09	13-sep-08	14-sep-09
Maíz	16-dic-08	03-dic-09	18-dic-08	19-dic-09
Soja	26-ene-09	29-ene-10	02-feb-09	02-feb-10
Soja de segunda	22-mar-09	25-mar-10	22-mar-09	22-mar-10

Las imágenes Landsat 5 TM se corrigieron atmosféricamente según el modelo propuesto por Chávez (1996) y se georreferenciaron con un error cuadrático medio menor a 15 m, utilizando una proyección Gauss-Krüger (faja 5), datum POSGAR 94. El producto MOD13Q1 de MODIS posee una proyección sinusoidal. Los datos MODIS fueron obtenidos en línea de NASA Land Processes Distributed Active Archive Center (LP DAAC), USGS/Earth Resources Observation and Science (EROS) Center, Sioux Falls, South Dakota (http://lpdaac.usgs.gov/get_data).

RESULTADOS

La campaña 2008/09 se caracterizó por una fuerte sequía que afectó a la región pampeana observándose una importante disminución de las precipitaciones. Promediando los datos de las siete EMA se puede apreciar que durante 2008, sólo el mes de julio presentó una leve anomalía positiva en las precipitaciones con respecto al promedio histórico. En este año, se produjeron precipitaciones un 52% menor a dicho promedio.

En cambio, en la campaña 2009/10 se registró una mayor cantidad de precipitaciones, aproximadamente 20% más que el promedio histórico durante 2009 (Figura 3). Entre septiembre de 2008 y enero de 2009 se registró una disminución de las precipitaciones algo mayor al 40 % comparado con el promedio histórico para la zona. En cambio, en la campaña 2009/10 se registraron precipitaciones de aproximadamente un 70 % mayor para el período septiembre-marzo.

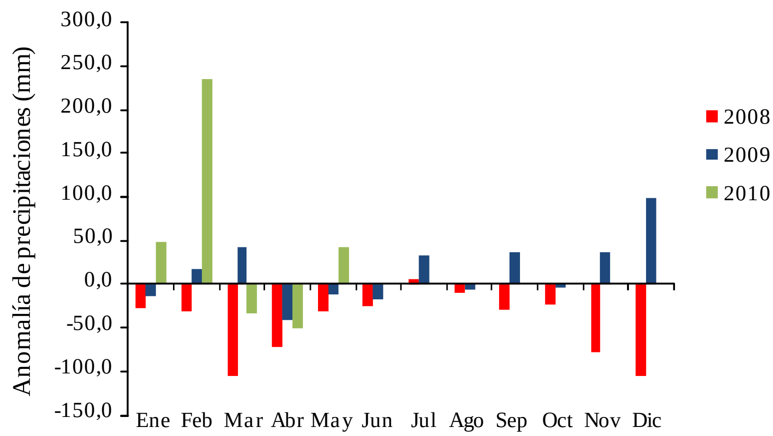

Figura 3. Anomalía de las precipitaciones en las campañas agrícolas 2008/09 y 2009/10 (Elaboración propia con datos de la Dirección de Hidráulica de Entre Ríos)

Vaiman (2011) encontró que la evolución temporal del NDVI de Landsat podía diferenciar el vigor de la vegetación entre campañas con marcadas diferencias en la cantidad de precipitaciones producidas durante el ciclo de los cultivos (Figura 4). Gran parte de estas variaciones en los valores de NDVI pueden explicarse por las variaciones de las condiciones climáticas (Jinyoung et al., 2010).

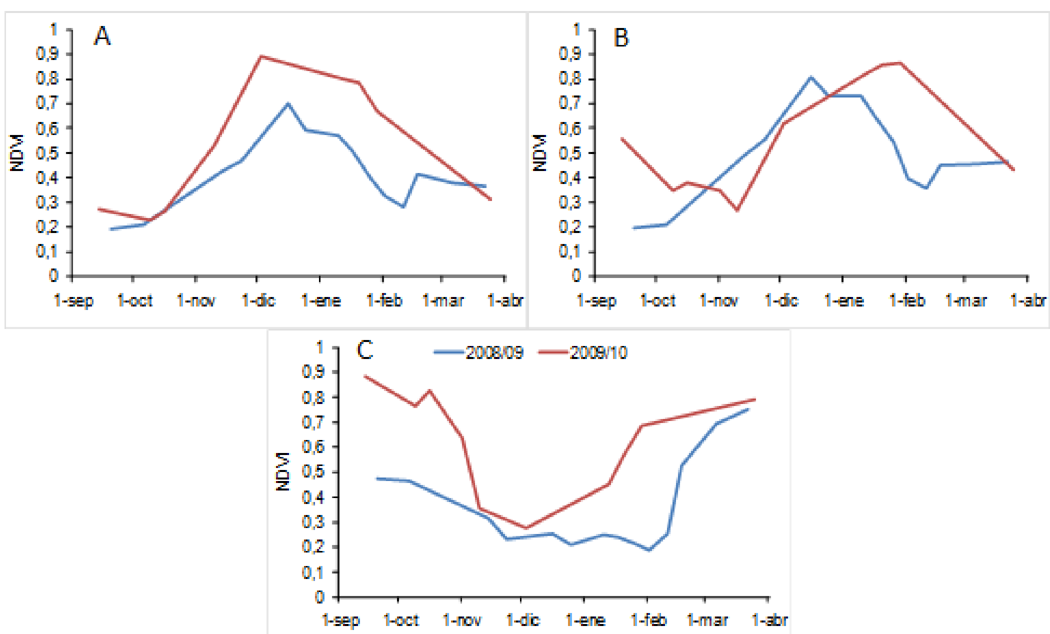

Figura 4. Evolución del NDVI en ambas campañas. Referencias: A: maíz; B: soja; C: trigo/soja

Los valores de NDVI presentaron diferencias significativas entre campañas para ambos sensores, excepto para Landsat en soja de segunda (Tabla 2). Los valores mayores se obtuvieron en la campaña más húmeda (2009/10) en todos los cultivos. Los valores hallados en maíz en dicha campaña son superiores a los citados por Marini (2008) y Dediós et al. (2001). En soja, los valores de NDVI son similares a los mencionados por Jackson et al. (2004), quienes citan valores máximos de 0,9 en cultivos de soja con un elevado índice de área foliar y, en cambio, mencionan valores bajos de NDVI para cultivos con escaso desarrollo foliar. Esta situación es esperable por los efectos de una menor turgencia a nivel celular lo que afecta la expansión de las hojas cuando las plantas se someten a estrés hídrico (Pandey et al., 1984; Cox y Joliff, 1986). En trigo, Epinat et al. (2001) citan valores de NDVI de 0,92 para trigo en un año húmedo. Este valor es similar al hallado en este trabajo en trigo durante la campaña húmeda.

Tabla 2. Comparación de valores de NDVI entre campañas para imágenes Landsat y MODIS

		Campaña 2008/09	Campaña 2009/10
NDVI Landsat*	Maíz	0,70 b	0,89 a
	Soja	0,54 b	0,87 a
	Trigo	0,47 b	0,88 a
	Soja de segunda	0,75 a	0,79 a
NDVI MODIS*	Maíz	0,62 b	0,79 a
	Soja	0,52 b	0,84 a
	Trigo	0,46 b	0,83 a
	Soja de segunda	0,66 b	0,84 a

* Letras distintas en sentido de las filas indican diferencias significativas ($p < 0,05$; $n = 30$)

Por otro lado, al comparar entre sensores para una misma campaña ($p < 0,05$; $n = 30$), los valores de NDVI en maíz y en soja de segunda presentaron diferencias significativas, en trigo existieron diferencias significativas solo en la campaña 2009/10, y en soja no se encontraron diferencias significativas entre ambos sensores. En todos los casos excepto en soja de segunda en la campaña 2009/10, los valores de NDVI provenientes de imágenes Landsat resultaron superiores a los de MODIS.

Los valores de NDVI de Landsat también resultaron superiores a los del sensor AVHRR de NOAA (Soria-Ruiz y Granados- Ramírez, 2005).

Los coeficientes de determinación hallados en la correlación entre los valores de NDVI del satélite Landsat y del MODIS resultaron elevados (Figuras 5 y 6).

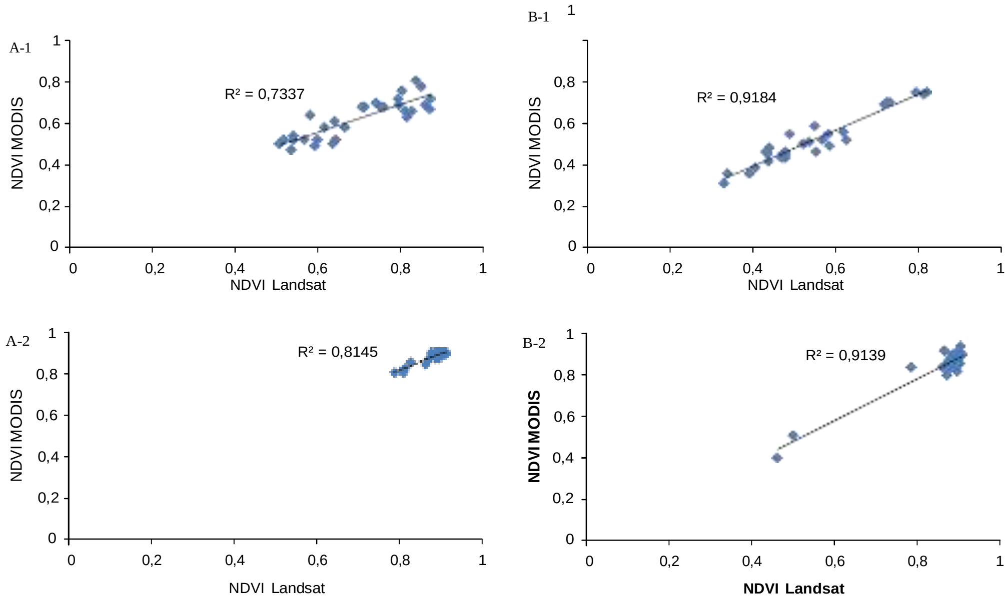

Figura 5. Correlación entre valores de NDVI de Landsat y de MODIS. Referencias: A: maíz, B: soja; 1: campaña 2008/09, 2: campaña 2009/10

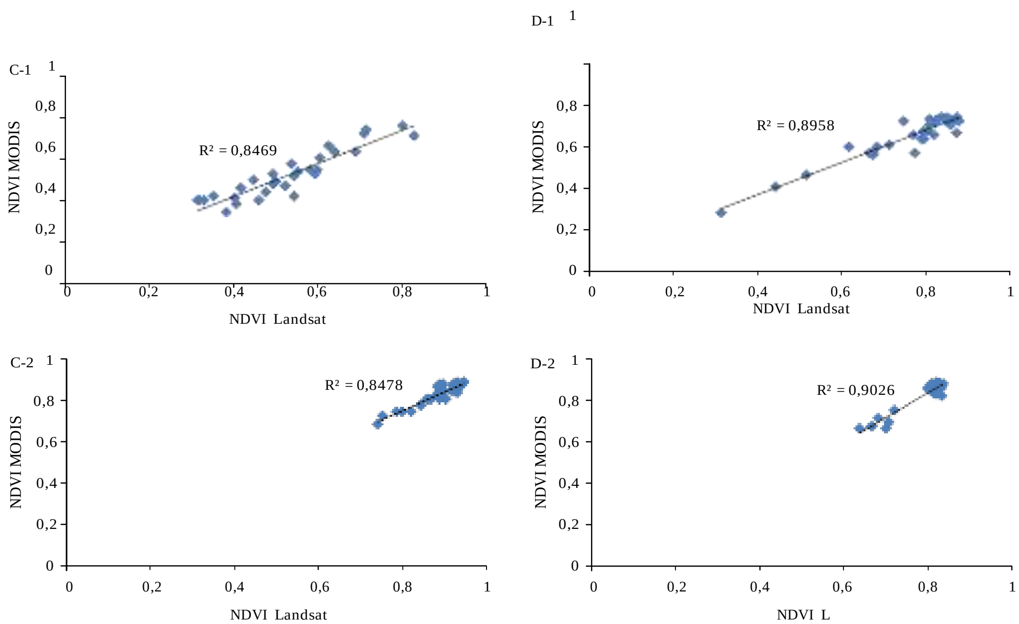

Figura 6. Correlación entre valores de NDVI de Landsat y de MODIS. Referencias: C: trigo, D: soja de segunda; 1: campaña 2008/09, 2: campaña 2009/10

CONCLUSIONES

Ambos sensores fueron capaces de detectar la diferencia en el vigor de los cultivos entre campañas, lo cual se explica por el déficit hídrico que sufrieron los cultivos en la campaña 2008/09 y las abundantes precipitaciones en la campaña 2009/10.
Las diferencias encontradas entre sensores se podrían explicar por la diferente resolución espectral de cada uno y porque el producto MOD13Q1 representa una integración de datos de una serie de tiempo, y no un dato puntual como en el caso de las imágenes Landsat.
La elevada correlación encontrada entre los datos de los dos sensores indicaría que ambos son adecuados para este tipo de estudio, pudiendo utilizarse uno u otro en base al nivel de detalle espacial requerido. Además, la mayor resolución espacial del sensor TM del Landsat discrimina con mayor eficiencia una cobertura de otra, y esto reduce la probabilidad de que se contamine la información con coberturas fronterizas.

AGRADECIMIENTOS

El trabajo fue realizado con fondos otorgados por la Agencia Nacional de Promoción Científica y Tecnológica de Argentina (PICT 06-1221) y la Universidad Nacional de Entre Ríos (PIDUNER 2128).

BIBLIOGRAFÍA

Chavez, P. S. 1996. Image-based atmospheric corrections – Revisited and improved. Photogrammetric Engineering and Remote Sensing 62 (9): 1025-1036.
Cox, W. J., Joliff, G. D. 1986. Growth and yield of sunflower and soybean under soil water deficits. Agron. J. 78: 226-230.
Dediós, N. J., García-Ferrer, A., Sánchez de la Orden, M. 2001. Detección de cubiertas vegetales en el área mediterránea. Aplicación del índice de vegetación en la subcuenca Genil Cordobilla. Teledetección, Medio Ambiente y Cambio Global, pp: 187-190.
Doraiswamy, P. C., Hatfield, J. L., Jackson, T. J., Akhmedov, B., Prueger, J., Stern, A. 2004. Crop condition and yield simulations using Landsat and MODIS. Remote Sensing of Enviroment 92: 548-559.
Epinat, V., Stein, A., de Jong, S. M., Bouma, J. 2001. A wavelet characterization of high-resolution NDVI patterns for precision agriculture. JAG 3 (2): 121-132.
Fischer, A. 1994. A model for the seasonal variations of vegetation indices in coarse resolution data and its inversion to extract crop parameters. Remote Sensing of Enviroment, 48: 220-230.
Hubbard, K. G. 1994. Spatial variability of daily weather variables in the high plains of the USA. Agric. For. Meteorol., 68: 29-41.
Jackson, T. J., Chen, D., Cosh, M., Li, F., Anderson, M., Walthall, C., Doriaswamy, P., Hunt, E. R. 2004. Vegetation water content mapping using Landsat data derived normalized difference water index for corn and soybeans. Remote Sensing of Environment, 92:475-482.
Ji, L., Peters, A. J. 2003. Assessing vegetation response to drought in the northern Great Plains using vegetation and drought indices. Remote Sens. Environ., 87: 85-98.
Jinyoung, R., Jungho, I., Carbone, G. J. 2010. Monitoring agricultural drought for arid and humid regions using multi-sensor remote sensing data. Remote Sensing of Environment, 114: 2875-2887.
Johnson, G.E., Achutuni, V. R., Thiruvengadachari, S., Kogan, F. 1993. The role of NOAA satellite data in drought early warning and monitoring: selected case studies. En: Wilhite, D.A. (Ed), Drought Assessment, Management, and Planning: Theory and Case Studies. Kluwer Academic, pp. 31-49.
Kyllo, K. P. 2003. NASA funded research on agricultural remote sensing, Department of Space Studies, University of North Dakota.
Marini, M. F. 2008. El avance de la frontera agrícola en el área adyacente al sistema Sierras de la Ventana (Buenos Aires, Argentina). Investigaciones Geográficas, 47: 111-121.
Mc Kee, T.B., N.J. Doesken y J. Kleist, 1995. Drought monitoring with multiple time scales. In: Proceedings of the 9th Conference on Applied Climatology. AMS, Boston, MA, pp 233-236.
Pandey, R. K., Herrera, W. A. T., Villegas, A. N., Pedleton, J. W. 1984. Drought response of grain legumes under irrigation gradient: III. Plant growth. Agron. J. 76: 557-560.
Rencz, A. N. 1999. Manual of remote sensing. Remote sensing for the Earth sciences (Volume 3). 3º Edition. American Society for Photogrammetry and Remote Sensing. 707 pp.
Rotondo, V. H., Seiler, R. A. 2001. Red agrometeorológica, mediciones y representatividad espacial para la caracterización del clima regional: Un caso de estudio para el Sur de Córdoba. Rev. Arg. de Agrometeorol., 1(2): 95-99.

Soria-Ruiz, J., Granados-Ramírez, R. 2005. Relación entre los índices de vegetación obtenidos de los sensores AVHRR del satélite NOAA y TM del Landsat. Ciencia ergo sum 12 (2): 167-174.

Thiam, A., Eastman, J. R. IDRISI Andes. Guide to GIS and image processing. Manual Version 15.00. Capítulo 18: Índices de vegetación. pp: 218-230. Clark University, Worcester Massachusetts.

Vaiman, N., 2011. Utilización de datos Landsat 5 en análisis multitemporal de cultivos, en situación normal y de sequía, en la zona centro Oeste de Entre Ríos. FCA UNER.

Yang, C., Bradford, J. M., Wiegand, C. L.2001. Airborne Multispectral imagery for mapping variable growing conditions and yields of cotton, grain sorghum, and corn. Transactions of the ASAE, 44 (6): 1983-1994.

Zang, P., Anderson, B., Tan, B., Huang, D., Myneni, R. 2005. Potential monitoring of crop production using a setellite-based Climate-Variability Impact Index. Agric. For. Meteorol., 132: 344-358.

Geoprocessamento aplicado à análise ecoepidemiológica da Doença de Chagas nos municípios de Abaetetuba e Barcarena, no Estado do Pará, Brasil, entre 2000-2011

Ricardo J. P. S. Guimarães 1; Alcinês S. Sousa Junior 1; Alcione F. Pinheiro 2; Rodrigo S. Dias 3; Fabrício A. Dias 1; Andréa Lívia Lins Neves 1; Irilene S. Souza Vale 4; Vera R. C. M. Palácios 3 e Nelson G. Veiga 2

1. Instituto Evandro Chagas - IEC/SVS/MS
Rodovia BR-316 km 7 s/n - 67030-000 - Ananindeua/PA, Brasil
2. Universidade Federal Rural da Amazônia - UFRA
3. Universidade do Estado do Pará - UEPA
4. Faculdade Estácio de Sá - Polo FAP
ricardojpsg@gmail.com

ABSTRACT

Chagas' disease whose incidence is conditioned to the presence of infected triatomines by *Trypanosoma cruzi* is a very big public health problem in the Brazilian Amazon region. Information on the eco- epidemiologic dynamics of vectors of diseases is needed to construct scenery of climate changes that have been noticed worldwide and related to antropic/local changes in the environment. The main propose of this work is to demonstrate the relationship between environmental degradation processes with the incidence of Chagas' disease in the municipalities of Abaetetuba and Barcarena, in the period 2000 to 2011. An environmental characterization using classified images of the Prodes and TerraClass Project. Abaetetuba showed a higher rate of deforestation and also an increased number of cases of Chagas disease. The rate of population increase, which was observed in the municipalities studied, too, can be a factor in increased deforestation and growth of cases of Chagas disease. Data from Prodes and TerraClass Project demonstrated the existence of a process of deforestation in the study area. The use of Geographic Information Systems with data from the Information System for Notifiable Diseases proved to be a very efficient tool to characterize the processes of environmental degradation that has occurred in the municipalities of Abaetetuba and Barcarena during the study period from 2000 to 2011.

Palavras-chave: geographic information system, schistosomiasis, *Biomphalaria*, sistema de informações geográficas, esquistossomose, *Biomphalaria*

1. INTRODUÇÃO

Doença de Chagas, cuja incidência está condicionada à presença de triatomíneos infectados por *Trypanosoma cruzi* é um problema de saúde pública muito grande na região amazônica brasileira.
Os vetores da doençade Chagas (DC) são insetos de orden *Hemiptera*, subfamilia *Triatominae* e conhecidos popularmente no Brasil como barbeiro. Estes insetos possuem habito alimentar hematófago (Lent & Wigodzinsky, 1979; Sandoval et al., 2000).
A doença de Chagas e considerada uma doença tropical, endêmica em certas regiões do Brasil e em outros 20 países da America Latina (Clayton, 2010). A doença de Chagas afeta cerca de 10 milhões de pessoas em países latino-americanos endêmicos. No Brasil, estima-se que cerca de um milhão e novecentas mil pessoas possuam o mal de Chagas (Rassi-Junior et al., 2010).
Na década de 60, foi relatado o primeiro surto agudo da doença de Chagas na Amazônia brasileira. Foi descrito no estado do Pará e as investigações não encontraram triatomíneos na área, propondo ser outra forma a via de transmissão. Segundo Valente et al. (2009) cerca de 600 novos casos agudos da DC foram registrados na Amazônia brasileira.

Nos últimos anos, vários surtos agudos da DC na Amazônia têm sido descritos, muitos desses associados à ingestão do vinho do açaí (*Euterpe oleracea*) (Valente et al., 1999, 2009; Coura Jr., 2006; Nobrega et al., 2009, Pereira et al., 2009).

Em função destes surtos e outros demais na Amazônia, o Programa Nacional de Controle de Doença de Chagas, da Secretaria de Vigilância em Saúde (PNCDCh/SVS), vem implantando desde novembro de 2005, um modelo de vigilância epidemiológica específico para a Região Amazônica (Brasil, 2006).

Estudos demonstram que a taxa anual de desmatamento na Amazônia brasileira e cerca de dois milhões de hectares. De 1988 até 2010 aproximadamente 385.234km^2 foram desmatados na Amazônia legal. Neste mesmo período, o estado do Pará foi o segundo estado com o maior índice de desmatamento no Brasil com uma taxa média de 5.543km^2, perdendo apenas para o estado de Mato Grosso com 5.834km^2 (Brasil, Projeto Prodes, 2012). Segundo Romana (2007) a transmissão de doenças por vetores está associada com as mudanças da cobertura vegetal, particularmente com o desmatamento.

O atual cenário da Amazônia brasileira configura no intenso fluxo migratório de pessoas procedentes de áreas endêmicas, no desmatamento descontrolado, na grande diversidade encontrada de *T. cruzi*, de hospedeiros vertebrados e espécies de triatomíneos (Aguilar et al., 2007).

O uso de ferramentas de geoprocessamento vem sendo amplamente utilizado em estudos na área de saúde, especialmente em pesquisas relacionadas com doenças tropicais. Com o uso destas ferramentas é possível fazer uma análise da distribuição geográfica das espécies, usando modelos de nichos ecológicos, assim como, avaliar o risco de infecção às populações e o seu controle.

Sistemas de Informação Geográfica (SIG) são úteis nos estudos de doenças. Em geral, o desmatamento de grandes áreas rurais interferirem com o potencial vetor, infecção de *T. cruzi* e de reservatórios de mamíferos, e que são desconhecidos para a região ao longo dos anos. Informações sobre a dinâmica ecoepidemiológica de vetores de doenças são necessário para construir cenários de mudanças relacionadas às alterações antrópicas. Desta forma, é possível avaliar as condições favoráveis para a dispersão dos vetores, bem como o seu desenvolvimento, o sucesso reprodutivo e a sobrevivência.

A principal proposta deste estudo é demonstrar a relação entre os processos de degradação ambiental com a incidência da doença de Chagas nos municípios de Abaetetuba e Barcarena, no período de 2000 a 2011.

2. METODOLOGIA DE TRABALHO

A área de estudo foi os municípios de Abaetetuba que localiza-se a uma latitude 01º43’05”S e a uma longitude 48º52’57”O, tem uma população de 147.846 habitantes em uma área de 1.617 km^2 e o município de Barcarena que localiza-se a uma latitude de em uma área de 1.315 km^2 (IBGE, 2012). Ambos os municípios estão localizados no nordeste do Estado do Pará e possui um clima equatorial super úmido (Figura 1).

Foram utilizadas imagens do satélite Landsat 223/61 e 224/61 (orbita/ponto) de 2000 a 2011, obtidas do Projeto Prodes (http://www.obt.inpe.br/prodes/index.html) e do Projeto Terra Class (http://www.inpe.br/cra/terraclass.php), para fazer o mapa da cobertura vegetal dos municípios estudados e comparar com os casos de Doença de Chagas obtidos da base de dados dos casos confirmados notificados no Sistema de Informação de Agravos de Notificação (SINAN). Foram obtidos 136 casos de pacientes positivos para a Doença de Chagas.

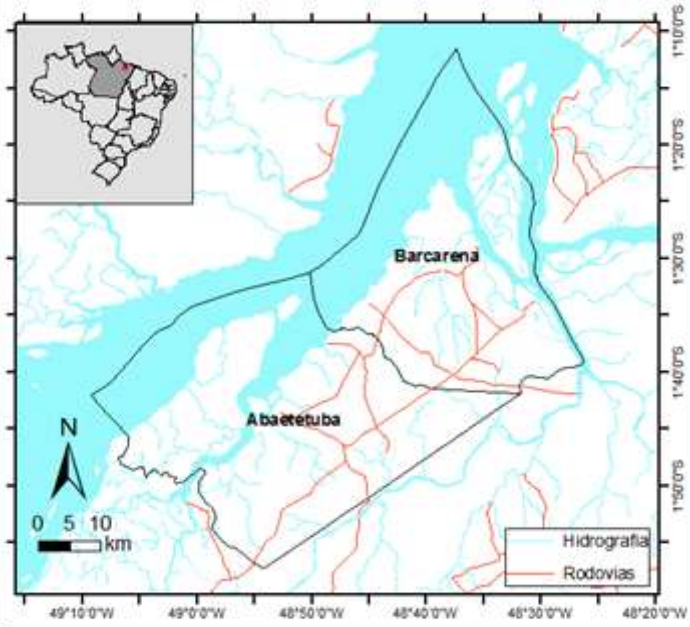

Figura 1. Localização espacial dos municípios de Abaetetuba e Barcarena

Foi desenvolvido um banco de dados com dados ecoepidemiológicos usando Sistemas de Informações Geográficas. Após o processo do banco de dados foram realizadas consultas espaciais, ligando a classificação do Projeto Prodes/TerraClass com os dados de Doença de Chagas nos municípios de Abaetetuba e Barcarena.

O software ArcGis (versão 9.3 – http://www.esri.com/) foi utilizado para as analises espaciais.

3. RESULTADOS E DISCUSSÃO

A Tabela 1 apresenta a quantidade de casos de pacientes positivos para a Doença de Chagas nos municípios de Abaetetuba e Barcarena, no período de 2000 a 2011.

Tabela 1. Casos de pacientes positivos para a Doença de Chagas no período de 2000 a 2011

Município	2000	2001	2002	2003	2004	2005	2006	2007	2008	2009	2010	2011
Abaetetuba	0	0	1	1	2	0	13	1	10	55	7	9
Barcarena	0	0	0	0	0	0	11	13	8	4	0	1

Observa-se na Tabela 1 que nos anos de 2000 e 2001 não houve casos de pacientes positivos para a Doença de Chagas, segundo dados do SINAN. Por isso, foram retirados das análises esses dois anos, assim como, não foram utilizadas as imagens classificadas do Projeto Prodes. A imagem classificada do Projeto Prodes do ano de 2011 pode ser visualizada na Figura 2.

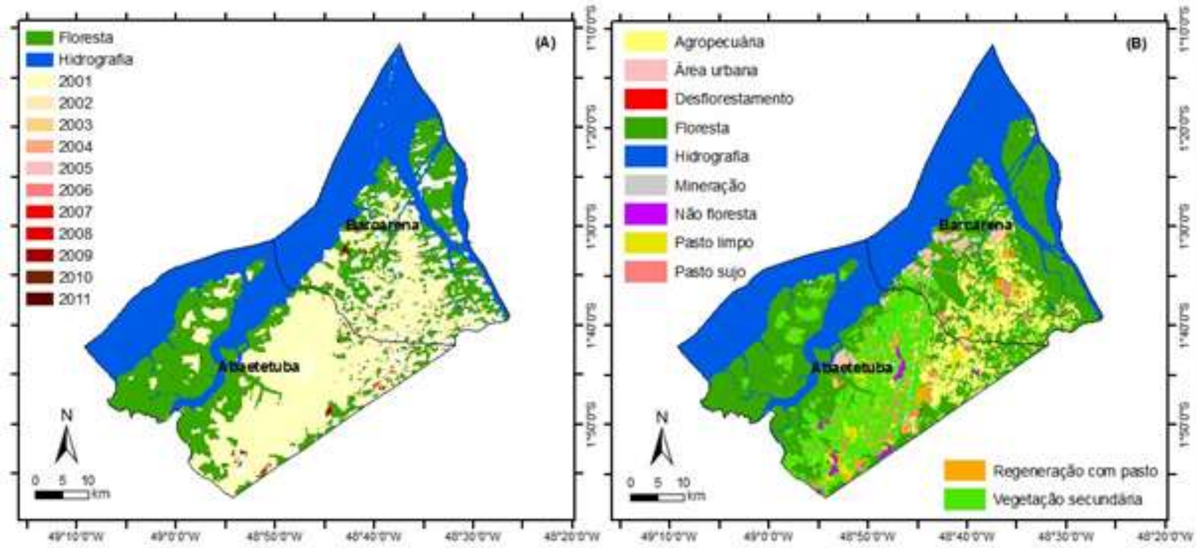

Figura 2. Imagens classificadas do projeto Prodes dos municípios de Abaetetuba e Barcarena nos anos de: (a) Classificação do Projeto Prodes e (b) Classificação do Projeto TerraClass

Dados dos Projetos Prodes (Figura 2A) e TerraClass (Figura 2B) demonstram a existência de um processo de desmatamento na região de estudo. A Figura 2(A) mostra o mapa de desmatamento da área de estudo do ano de 2011 com os incrementos de desmatamento dos anos de 2001 a 2011. Observa-se na Figura 2(A) que existe um processo de degradação ambiental mais elevado no município de Abaetetuba do que em Barcarena.

A Figura 2(B) mostra a classificação do Projeto TerraClass do ano de 2008, onde observa-se que Abaetetuba e Barcarena apresentam uma grande área agrícola. Também, nota- se que Abaetetuba tem uma grande área de vegetação secundária, além de várias áreas de regeneração com pasto.

Ao longo da história de análise de desmatamento da Amazônia Legal pelo Projeto Prodes (Brasil, Projeto Prodes, 2012), a quantidade de desmatamento de Abaetetuba foi de 42,68%, o que representa quase o dobro do ocorrido no município de Barcarena que foi de 24,71%, além do fato de Abaetetuba possuir uma população de 141.100 habitantes, que representa cerca de 40% a mais do que Barcarena que tem 99.859 habitantes (IBGE 2012), esse fato pode ter contribuído para o processo de transmissão da DC.

Tabela 2. Porcentagem de desmatamento obtido do Projeto Prodes nos municípios estudados no período de 2002 a 2011

Município	2002	2003	2004	2005	2006	2007	2008	2009	2010	2011
Abaetetuba	0,16	0,15	0,7	0,2	0,28	0,25	0,08	0,19	0,24	0,05
Barcarena	0,56	0,75	0,69	0,29	0,52	0,25	0,09	0,21	0,14	0,08

Por outro lado, na Tabela 2 observa-se que no período de estudo (2002 a 2011) ao contrário do processo de desmatamento citado no parágrafo acima, Barcarena sofreu um maior desmatamento do que Abaetetuba, cerca de 3,6% e 2,3%, respectivamente, dados esses também obtidos do Projeto Prodes (Brasil, Projeto Prodes, 2012). Este fato pode estar relacionado com a criação do polo industrial de Barcarena e, também, segundo o IBGE (2012) a população de Abaetetuba cresceu cerca de 20% nos últimos 10 anos (censo 2000 e 2010) e Barcarena cresceu cerca de 57%.

4. CONCLUSÕES

A utilização dos Sistemas de Informação Geográfica (SIG) com os dados obtidos do Sistema de Informação de Agravos de Notificação (SINAN) mostrou ser uma ferramenta muito eficiente para caracterizar os processos de degradação ambiental que ocorreu nos municípios de Abaetetuba eBarcarena, no período estudado de 2000 a 2011. Também, o SIG demonstrou ser um poderoso recurso para captar, armazenar e recuperar informações.

A classificação utilizando imagens digitais possibilitou visualizar nas áreas de estudos as características ambientais propícias à propagação da doença de Chagas.

Os resultados obtidos do Projeto Prodes e do IBGE sugerem a possibilidade que a ocorrência da DC tenha sido influenciada por alterações induzidas pelo homem no meio ambiente.

Também, os resultados mostraram que o município de Abaetetuba apresentou maior desmatamento do que no município de Barcarena e isso pode ser a causa do aumento de casos de doença de Chagas apresentados em Abaetetuba. Dias (2011) estudou a transmissão de doença de Chagas nas localidades de São Tomé, Araipá e Nova Estrela pertencentes ao município de Aveiro/PA e também mostrou a relação entre desmatamento e DC.

A taxa de crescimento populacional, que foi observada nos municípios estudados, também, pode ser um fator para o aumento do desmatamento e do crescimento de casos de doença de Chagas.

Serão obtidos os dados de DC do banco de dados do IEC para uma comparação, validação e, também, para a obtenção das coordenadas das localidades/endereços dos pacientes positivos para a Doença de Chagas. Essas coordenadas serão georreferenciadas com o uso de um aparelho GPS e depois analisadas com os dados das imagens do Projeto Prodes para uma melhor identificação do tipo de uso do solo associado com a incidência da doença.

AGRADECIMENTOS

A Universidade do Estado do Pará (UEPA), Laboratório de Geoprocessamento do Instituto Evandro Chagas (LabGeo/IEC) e Secretaria Municipal de Saúde (SESMA).

REFERÊNCIAS BIBLIOGRÁFICAS

Aguilar, H.M.; Abad-Franch, F.; Dias, J.C.P.; Junqueira, A.C.V.; Coura, J.R.. Chagas disease in the Amazon region. Mem Inst Oswaldo Cruz, v. 102 (Suppl. 1), p. 47-55. 2007.

Brasil. Ministério da Saúde. 2006. Surto de Doença de Chagas Agudo (DCA) em Santarém/Para - junho de 2006. Disponível em:<http://portal.saude.gov.br/portal/saude/visualizar_texto.cfm?idtxt=24541>. Acessado em: 01 de out. de 2012.

Brasil. Ministério da Ciência e Tecnologia. Projeto Prodes - Monitoramento da Floresta Amazônica Brasileira Por Satélite. Disponível em:<http://www.obt.inpe.br/prodes/index.html>. Acessado em: 01 de out. de 2012. Clayton, J. Chagas disease 101. Outlook Chagas Disease, Nature, S4-S5. 2010

Coura, J.R.. Transmissão da infecção chagásica por via oral na historia natural da doença de Chagas. Rev Soc Bras Med Trop, v. 39 (Supl. IV) p. 113-117. 2006

Dias, F.B.S. Aspectos ecológicos da Tripanossomíase Americana em comunidades do médio Tapajós, Pará, Brasil, e riscos de transmissão do *Trypanosoma cruzi* às populações humanas da região. 2011. 191 p. Tese (Doutorado em Doenças Infecciosas e Parasitárias) - Centro de Pesquisas René Rachou, Belo Horizonte. 2011.

IBGE (Instituto Brasileiro de Geografia e Estatística). Censo Demográfico 2010. Disponível em: <http://www.sidra.ibge.gov.br/bda/tabela/protabl.asp?c=137&z=t&o=7&i=P Acessado em: 03 out. de 2012.

Lent, H.; Wygodzinsky, P. Revision of the *Triatominae* (*Hemiptera*, *Reduviidae*), and their significance as vectors of Chagas' disease. Bull Amer Mus Nat Hist, v. 163. New York. 1979.

Nobrega, A.A.; Garcia, M.H.; Tatto, E.; Obara, M.T.; Costa, E.; Sobel, J.; Araujo, W.N.: Oral Transmission of Chagas Disease by Consumption of Açai Palm Fruit, Brazil. Emerging Infec Disease, v. 15 p. 653-655. 2009.

Pereira, K.S.; Schmidt, F.L.; Guaraldo, A.M.; Franco, R.M.; Dias, V.L.; Passos, L. A. Chagas' disease as a foodborne illness. J Food Prot. v. 72, p. 441-446. 2009.

Rassi, J.R.A.; Rassi, A.; Marin-Neto, J.A. Chagas disease. Lancet, v. 375, p. 1388-1402. 2010.

Romana, C. O controle da tripanossomíase americana requer vigilância ecológica e social da emergencia de risco. In: Teixeira ARL, Doença de Chagas e Evolução. Ed. UnB. Brasília, cap. 17, p. 233-251. 2007.

Sandoval, C.M.; Joya, M.I.; Gutierrez, R.; Ângulo, V.M. Cleptohaematophagy of the triatomine bug *Belminus herreri*. Med Vet Entomology, v. 14, p. 100-101. 2000.

Valente, S.A.S.; Valente, V.C.; Fraiha NETO, H. Considerations on the epidemiology of Chagas disease in the Brazilian Amazon. Mem Inst Oswaldo Cruz, v. 94 (Suppl. 1), p. 395-398. 1999.

Valente, S.A.S.; Valente, V.C.; Pinto, A.Y.N.; Cesar, M.J.B.; Santos, M.P.; Miranda, C.O.S.; Cuervo, P.; Fernandes, O. Analysis of an acute Chagas disease outbreak in the Brazilian Amazon: human cases, triatomines, reservoir mammals and parasites. Trans Royal Soc Trop Med Hyg, v. 103, p. 291-297, 2009.

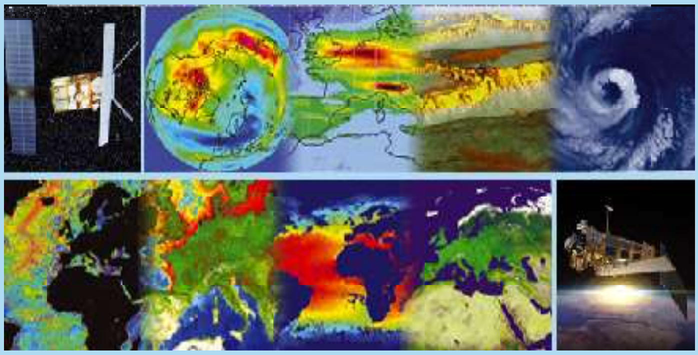

ESA promueve el desarrollo y la cooperación internacional

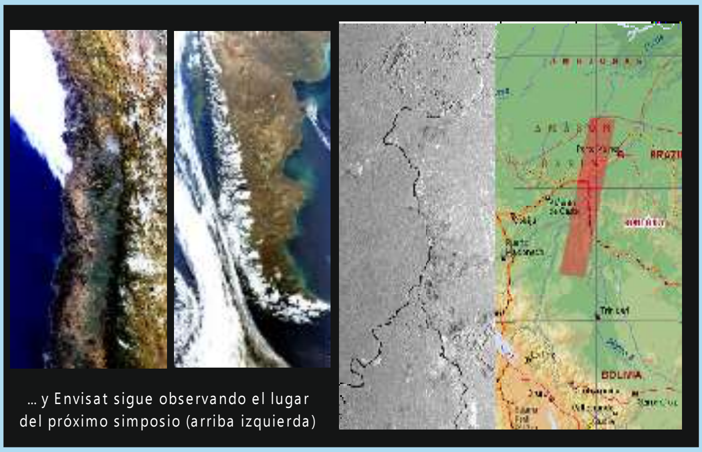

... y Envisat sigue observando el lugar del próximo simposio (arriba izquierda)

ESA - ESRIN
Via Galileo Galilei,
Casella Postale 64.
00044 Frascati (Roma)
ITALIA
Tel: (39.06) 94180.409
Fax: (39.06) 94180.280
Att: Sr. Francesco Sarti (América Latina)

ESA - Asuntos Internacionales
8-10 rue Mario Nikis,
75738 PARIS Cedex 15, FRANCIA
Tel: (33.1) 5369.7731, Fax: (33.1) 5369.7627
Att: Sra. Marie Elisabeth De Vel (América Latina)

ECUADOR 1980 - 1983 | CHILE 1983 - 1986 | BRASIL 1986 - 1989 | ARGENTINA 1989 - 1991 | PERU 1991 - 1993 | COLOMBIA 1993 - 1995 | MEXICO 1995 - 1997 | VENEZUELA 1997 - 1999 | ARGENTINA 2000 - 2002 | BOLIVIA 2002 - 2004 | CHILE 2004 - 2006 | COLOMBIA 2006 - 2008 | CUBA 2008 - 2010 | MEXICO 2010 - 2012 | GUYANA FRANCESA 2012 - 2014